Liver Fibrosis: Review of Current Imaging and MRI Quantification Techniques

Léonie Petitclerc, MSc,[1,2] Giada Sebastiani, MD,[3] Guillaume Gilbert, PhD,[1,4]
Guy Cloutier, PhD Eng,[1,2,5,6] and An Tang, MD, MSc[1,2,5]*

Liver fibrosis is characterized by the accumulation of extracellular matrix proteins such as collagen in the liver interstitial space. All causes of chronic liver disease may lead to fibrosis and cirrhosis. The severity of liver fibrosis influences the decision to treat or the need to monitor hepatic or extrahepatic complications. The traditional reference standard for diagnosis of liver fibrosis is liver biopsy. However, this technique is invasive, associated with a risk of sampling error, and has low patient acceptance. Imaging techniques offer the potential for noninvasive diagnosis, staging, and monitoring of liver fibrosis. Recently, several of these have been implemented on ultrasound (US), computed tomography, or magnetic resonance imaging (MRI). Techniques that assess changes in liver morphology, texture, or perfusion that accompany liver fibrosis have been implemented on all three imaging modalities. Elastography, which measures changes in mechanical properties associated with liver fibrosis—such as strain, stiffness, or viscoelasticity—is available on US and MRI. Some techniques assessing liver shear stiffness have been adopted clinically, whereas others assessing strain or viscoelasticity remain investigational. Further, some techniques are only available on MRI—such as spin-lattice relaxation time in the rotating frame ($T_1\rho$), diffusion of water molecules, and hepatocellular function based on the uptake of a liver-specific contrast agent—remain investigational in the setting of liver fibrosis staging. In this review, we summarize the key concepts, advantages and limitations, and diagnostic performance of each technique. The use of multiparametric MRI techniques offers the potential for comprehensive assessment of chronic liver disease severity.
Level of Evidence: 5

Liver fibrosis is characterized by the accumulation of extracellular matrix proteins as a result of repeated injury to the tissue due to chronic liver disease.[1] All causes of chronic liver disease—including viral hepatitis, metabolic, and cholestatic disease—may lead to fibrosis.[2]

Liver biopsy is the current reference standard for the diagnosis and staging of fibrosis. However, it is associated with the limitation of sampling error, as it only examines a small liver sample, has low patient acceptance, and low intra- and interobserver repeatability.[3,4] In recent years, efforts have been made to migrate toward noninvasive techniques for assessing liver fibrosis.

Several imaging techniques have been developed for the diagnosis and staging of liver fibrosis. Historically, clinicians and radiologists have relied on the assessment of morphological changes associated with liver fibrosis. Other techniques rely on changes in physical properties that can be assessed quantitatively with imaging methods. These include texture, mechanical properties, $T_1\rho$ lengthening, diffusion, perfusion, and hepatocellular function. Elastographic techniques implemented on commercial ultrasound (US) and magnetic resonance imaging (MRI) systems have gained the widest clinical acceptance in the context of liver fibrosis imaging. The others are mainly restricted to an investigational setting.

The most widely validated and used liver fibrosis staging techniques are US-based elastography techniques. These techniques have improved the management of liver diseases by providing an alternative to liver biopsy. Moreover, many MRI techniques for imaging of liver fibrosis are being

FIGURE 1: Biopsy samples staged 0 to 4 according to the Brunt scoring system based on the use of Masson trichrome stain (5×–10× magnification). 0: no fibrosis; 1: mild zone 3 perisinusoidal fibrosis; 2: zone 3 perisinusoidal fibrosis, portal and periportal fibrosis; 3: bridging fibrosis; and 4: cirrhosis[12]. Figure courtesy of Dr. Bich Nguyen, University of Montreal.

developed. These MRI-based techniques have potential advantages over US elastography that will be discussed and may play an important role in the future.

This article will first describe the clinical features of liver fibrosis. Imaging-based techniques developed for the staging of liver fibrosis will then be discussed, with an emphasis on MR-based techniques.

Liver Fibrosis: Overview

Pathophysiology

Liver fibrosis occurs when there is an excessive accumulation of extracellular matrix proteins, resulting from the imbalance between deposition and removal of proteins such as collagen, laminin, elastin, and fibronectin. It is a ubiquitous wound-healing response to an acute or chronic injury.[5] Hepatic stellate cells, which are quiescent in the absence of inflammatory stimuli, undergo activation in response to liver injury, which may lead to fibrotic scarring and eventually to liver cirrhosis.[6] Other cell types have been associated with the development of fibrosis, such as myofibroblasts.

Epidemiology

Chronic liver diseases are a major cause of morbidity and mortality worldwide, affecting 360 per 100,000 persons and ranking as the 12th leading cause of overall mortality.[2] Pathologies leading to liver fibrosis are chronic viral hepatitis (hepatitis B, C, and delta), metabolic liver diseases (nonalcoholic fatty liver disease [NAFLD], alcoholic liver disease, primary and secondary hemochromatosis, Wilson's disease, and α1-antitrypsin deficiency), and cholestatic or autoimmune liver disease (primary biliary cholangitis, primary sclerosing cholangitis, autoimmune hepatitis). NAFLD is the most frequent liver disease in Western countries, affecting 10–30% of the general population.[7]

Complications

Independent of etiology, the accumulation of fibrosis in the liver is a common histopathological pathway, with the greatest impact on the prognosis of chronic liver diseases. If left untreated, liver fibrosis may evolve to its endstage of cirrhosis, which is associated with a high risk of developing hepatocellular carcinoma (HCC) and liver failure.[8] Decompensation and endstage complications of liver cirrhosis decrease dramatically the life expectancy of patients. These complications include portal vein thrombosis, development of HCC, formation of esophageal varices, ascites, and hepatic encephalopathy. The only definitive treatment for decompensated liver cirrhosis is liver transplantation. Hence, early identification of patients at risk of developing liver cirrhosis and decompensated liver disease is critical to initiate therapy.

Diagnosis

Guidelines recommend liver fibrosis staging for all causes of chronic liver diseases to establish prognosis and guide management. Liver biopsy has long been the gold standard of reference to stage fibrosis in the liver.[3]

Liver Fibrosis Staging

Several liver fibrosis staging systems have been proposed according to the underlying disease. The METAVIR scoring system is widely used, particularly for hepatitis B and C.[9] The Ishak's system is a revised version of an older histological activity index mainly applied to hepatitis B and C.[10,11] The Brunt system applies specifically to NAFLD and nonalcoholic steatohepatitis (NASH).[12] These histological staging systems group all patients with cirrhosis into a single category, without taking into account the severity of cirrhosis. The Laennec staging system, a modification of the METAVIR system, was proposed to provide a more refined histological subclassification of cirrhosis.[13] This system subdivides cirrhosis into three groups (4A, 4B, and 4C) based on the thickness of the fibrous septa and the size of nodules.

Both the METAVIR and Brunt systems—arguably the most commonly used systems—stage liver fibrosis on a scale of 0–4 through visual assessment of the amount and distribution of fibrous tissue on histopathology slides (Fig. 1). While semiquantitative scoring systems differ in the number of categories, they distinguish the following stages: 0, absence of liver fibrosis; 1, mild fibrosis with portal fibrosis, defined as a stellate enlargement of portal tracts; 2, significant fibrosis with portal fibrosis and a few septa between

portal tracts or hepatic veins; 3, severe fibrosis with septal fibrosis; and 4, liver cirrhosis with diffuse fibrosis delineating regenerative nodules.

Advantages and Limitations of Liver Biopsy

Liver biopsy has several advantages, including direct evaluation of fibrosis stage, ability of performing several stains, and evaluation of coexisting disorders such as the presence of fat, iron, inflammation, biliary disease, and overlap conditions.[14,15]

However, fibrosis staging by liver biopsy also has limitations. Cirrhosis may be missed if the liver biopsy sample is inadequate.[16,17] Samples taken from both lobes of the liver may lead to differences of at least one fibrosis stage in 33.1% of cases due to disease heterogeneity.[18] Smaller samples lead to underestimation of the liver fibrosis stage.[19] Requirements regarding the size of liver biopsy samples and number of portal tracts vary in the literature.[20–23] However, bigger samples are favored.[24]

Further, liver biopsy is associated with complications that are intrinsic to its invasive nature. Pain is common, occurring in up to 84% of patients and predominantly related to percutaneous liver biopsy.[25] Bleeding constitutes a severe complication, especially when it takes place intraperitoneally, occurring in 1 in 2500 to 1 in 10,000 biopsies.[4] Studies have shown patients' and physicians' reluctance toward liver biopsy.[26,27] Finally, liver biopsy is costly, requires a trained physician, and often hospitalization.

Treatment of Liver Fibrosis

Fibrosis stage dictates the decision to treat and prioritization for intervention in patients at higher risk for fast progression to liver cirrhosis and endstage complications of chronic liver disease. Emerging evidence suggests that liver fibrosis is a dynamic and reversible process, thus it may be treated and its evolution reversed if detected in its early stages.[28] The presence of significant liver fibrosis (stage ≥ 2), is considered a definitive indication for treatment. This threshold is clinically meaningful because it is the hallmark of a progressive liver disease, which eventually progresses to liver cirrhosis. Identification of cirrhosis (stage 4) is also pivotal in clinical practice since it requires a specific management, including screening for HCC and for esophageal varices.[29,30]

Monitoring of Liver Fibrosis

Upon finding liver fibrosis, there is a need to monitor disease progression over time. However, using repeated biopsies for this purpose would be unrealistic because of the costs and risks associated with the procedure.[26] Hence, the use of noninvasive techniques would be more acceptable for monitoring of disease stage.

TABLE 1. Overview of Imaging Techniques for Assessment of Liver Fibrosis

Techniques	Imaging modalities		
	US	CT	MRI
Morphology	Yes	Yes	Yes
Texture	Yes	Yes	Yes
Elastography	Yes	No	Yes
Strain imaging	Yes[a]	No	Yes
T1ρ	No	No	Yes
Diffusion-weighted imaging	No	No	Yes
Perfusion	Yes	Yes	Yes
Hepatocellular function	No	No	Yes

"Yes" indicates that the technique has been implemented on the corresponding imaging modality and "No" indicates that the technique is not available on this modality.
[a]Although strain imaging is available on the ultrasound systems, this technique is not used for the assessment of liver fibrosis.

Imaging of Liver Fibrosis

Table 1 provides an overview of techniques implemented with each imaging modality. MR can evaluate several tissue contrast mechanisms not available with other imaging modalities.

We review the imaging of liver fibrosis according to changes in physical or physiological properties. Whenever applicable, we provide a brief overview of US- and computed tomography (CT)-based techniques before focusing on MR-based methods. For each approach, we summarize the key concepts, advantages and limitations, and diagnostic performance. Diagnostic performance is reported for studies which use histopathology as their reference standard, unless otherwise stated. The area under the receiver operating characteristic curve (AUC) was available for most techniques. However, except for elastography, sensitivity and specificity with the associated diagnostic thresholds were seldom reported in the literature.

Comparison of MRI Techniques

The relative strengths and limitations of MRI-based techniques for assessment of liver fibrosis are summarized in Table 2. The diagnostic performance of MRI techniques is summarized in Table 3.

Morphology

Concept

Radiological investigation of the liver may reveal morphological features of cirrhosis. Some visible signs of cirrhosis include a nodular contour of the liver, segmental atrophy, blunt edges, widened fissures, expanded gallbladder fossa, and right posterior hepatic notch.[31,32] As cirrhosis leads to

TABLE 2. Advantages and Limitations of MRI-Based Imaging Techniques

Techniques	Advantages	Limitations
Morphology	- Simple - Widely available - No postprocessing required	- Subjective - Low repeatability - Not sensitive for early fibrosis
Texture	- Can be performed on any modality - Can be performed on routine clinical images	- Requires postprocessing software - Dependent on image quality
Elastography	- MRE has the highest diagnostic performance for staging liver fibrosis	- Several biological and technical confounders - Requires additional hardware - Requires postprocessing
Strain imaging	- No additional hardware required - Assesses the left liver lobe (hence may complement MRE)	- Requires postprocessing - Diagnostic performance not well validated
T1ρ	- No additional contrast agent or hardware required	- Increased sensitivity to B_0 and B_1 field inhomogeneities - High specific absorption rate - Recently introduced - Diagnostic performance not well validated
Diffusion-weighted imaging	- Widely available	- Technique not standardized - Sensitive to motion - Measurements often unreliable in left liver lobe - Conflicting results on relationship between ADC and fibrosis stage
Perfusion	- Potential prognostic significance	- Requires intravenous contrast agent - Requires postprocessing - Technique and modelling not standardized
Hepatocellular function	- Can be incorporated to clinical liver MRI examinations - Fast and simple postprocessing	- Additional cost related to hepatobiliary contrast agent - Validation required

ADC: apparent diffusion coefficient; MRE: magnetic resonance elastography.

portal hypertension, the following findings may become visible: splenomegaly, ascites, and varices.[31] These morphological features of cirrhosis have been assessed with US,[33–36] CT,[37–39] and MRI.[40,41] One study[42] performed a paired comparison of US-, CT-, and MRI-determined morphological changes for detection of liver fibrosis and found through ROC curve analysis that CT and MRI had marginally better diagnostic performance than US for the detection of cirrhosis. Some of these studies used a semiquantitative approach to the diagnosis of cirrhosis by using a radiologist-defined

score based on the appearance of some of the features listed above. Others use a more quantitative approach by measuring the length of liver segments or the spleen.[40]

Advantages and Limitations

Assessing morphological features for the diagnosis of cirrhosis is easy to perform and feasible on all three imaging modalities. However, the approaches used are mostly qualitative and have low repeatability, as the scoring of these imaging features is highly subjective. Also, it does not allow

TABLE 3. Summary of Diagnostic Performance of MRI-Based Techniques

Technique	Reference	Fibrosis stage ≥1			Fibrosis stage ≥2			Fibrosis stage ≥3			Fibrosis stage 4		
		AUC	Sn	Sp	AUC	Sn	Sp	AUC	Sn	Sp	AUC	Sn	Sp
Morphology	42	—	—	—	—	—	—	—	—	—	—	0.68-0.87	0.54-0.68
	40	—	—	—	—	—	—	—	—	—	—	0.93-1.00	0.13-0.93
	41	—	—	—	—	—	—	—	—	—	—	0.41-0.82	0.64-0.96
	170	—	—	—	—	—	—	—	—	—	0.84-0.95	0.77-0.88	0.75-0.89
Texture													
Nonenhanced	53	0.78-0.87	—	—	—	—	—	—	—	—	—	—	—
	57	0.53-0.60	—	—	—	—	—	—	—	—	—	—	—
SPIO enhanced	55	—	—	—	0.40-0.84	—	—	—	—	—	—	—	—
Gd enhanced	57	0.62-0.80	—	—	—	—	—	—	—	—	—	—	—
Double enhanced	55	—	—	—	0.82-0.89	—	—	—	—	—	—	—	—
	43	—	—	—	—	0.919	0.839	—	—	—	—	—	—
	56	0.814	0.659	0.8	0.889	0.895	0.778	0.862	0.778	0.784	0.976	1	0.93
Elastography[a]	96	0.95	0.83	0.99	0.98	0.94	0.95	0.98	0.92	0.96	0.99	0.99	0.94
	97	0.84	0.73	0.79	0.88	0.79	0.81	0.93	0.85	0.85	0.92	0.91	0.81
	98	0.94	0.87	0.93	0.97	0.87	0.94	0.96	0.87	0.92	0.97	0.93	0.91
T1ρ	114	—	—	—	—	—	—	0.97	—	—	0.97	1.00	0.84
Diffusion-weighted imaging[a]	96	0.86	0.81	0.82	0.83	0.77	0.78	0.86	0.72	0.84	—	—	—
Perfusion	141	—	—	—	—	—	—	0.61-0.82	0.31-0.92	0.64-1.00	—	—	—
	143	0.83	0.78	0.84	0.85	0.90	0.77	0.88	0.81	0.85	0.92	0.80	0.89
	133	—	—	—	—	—	—	—	—	—	0.57-0.95	0.50-1.00	0.50-1.00
Hepatocellular function	171	—	0.46	0.85	—	0.46	0.82	—	0.63	0.68	—	0.76	0.65
	149	0.81	0.70	0.85	0.82	0.75	0.77	0.85	0.73	0.87	0.83	0.83	0.80
	152	0.91	1.00	0.73	0.96	1.00	0.87	0.93	0.74	0.98	0.97	0.91	1.00
	151	0.82	0.87	0.75	0.68	0.75	0.56	0.63	0.75	0.50	0.62	0.82	0.49

AUC: area under the receiver operating characteristic curve; Sn: sensitivity; Sp: specificity; SPIO: superparamagnetic iron oxides.
Dash indicates that the data are not available.
Numbers indicate baseline value, whereas range reflect variety of acquisition parameters or analysis methods.
[a]Values reported from meta-analyses.

Normal   **Cirrhosis**

SD in ROI = 25	SD in ROI = 141
Entropy in ROI = 0.00	Entropy in ROI = 1.47
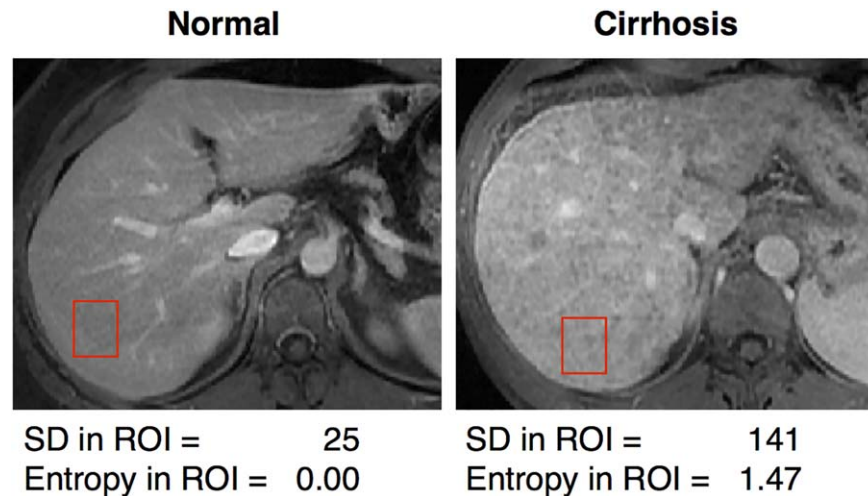
FIGURE 2: Examples of T_1-weighted fat-saturated contrast-enhanced MRI in a patient without known chronic liver disease and another with liver cirrhosis showing the altered texture of liver parenchyma affected by fibrosis. Note the higher standard deviation (SD) and higher entropy in regions of interest (ROIs) in the patient with cirrhosis (fibrosis stage 4).

for accurate staging of liver fibrosis and only has moderate accuracy for the diagnosis of cirrhosis.

Diagnostic Performance

Studies have found varying AUCs as low as 0.72[42] and as high as 0.91[35] for the diagnosis of stage 4 fibrosis (cirrhosis). The assessment of morphological features on liver MRI covers a wide range of sensitivity and specificity values (see Table 3) for detection of cirrhosis; however, this technique does not allow fibrosis staging.

Texture Analysis

Concept

Liver fibrosis leads to changes in the texture of the parenchyma. A fibrotic liver typically appears to have a coarser texture than healthy tissue.[43]

These changes may be assessed using computer-based texture analysis for quantitative measurement of the liver texture. Several analysis methods are used to extract a number of features from regions of interest in the image, such as histogram, co-occurrence matrix, and wavelet transform analysis.[43] Studies have used features individually or in combination for assessment of fibrosis stages. This concept has been applied to all three imaging modalities, and has been implemented both on unenhanced and contrast-enhanced imaging studies. The injection of contrast agents increases the visibility of fibrous tissue, which gradually enhances in the portal venous phase and becomes most conspicuous in the delayed venous phase. Further, this increases the contrast between late-enhancing fibrous tissue and cirrhotic nodules (Fig. 2).

On US, B-mode imaging[44–46] and contrast-enhanced US (CEUS)[47] have been used. On CT, some studies have used unenhanced images,[48] although most rely on contrast-enhanced images for texture analysis.[49–51] On MRI, several

sequences have been investigated for texture analysis, including unenhanced T_1-weighted,[52] T_2-weighted,[53] and proton density-weighted imaging.[54] Contrast-enhanced images have often been analyzed.[43,55–57] One interesting variant to contrast injection includes the use of double contrast-enhanced MRI images.[43,55,56] This is performed with the sequential injection of a gadolinium chelate and superparamagnetic iron oxides (SPIOs). The combined effect of these contrast agents accentuates the contrast between the fibrous tissue and cirrhotic nodules since gadolinium chelates cause delayed enhancement of the fibrotic region and SPIOs cause marked hypointensity of cirrhotic nodules due to T_2^* shortening. This double-contrast technique highlights the texture of liver parenchyma in the presence of fibrosis or cirrhosis. However, ferumoxides are no longer available, so some radiologists use ferumoxytol. This drug is not approved as a contrast agent, so its use for imaging is either investigational or off-label.[58]

Advantages and Limitations

Texture analysis may be carried out on any imaging modality and does not necessitate specialized hardware. Most imaging sequences, including routine clinical images, may be used for analysis. Many softwares are used and many features are reported for texture analysis. However, these techniques are not standardized, which makes comparison between studies challenging. The need for postprocessing software can also be a limitation. The results of texture analysis also strongly depend on the technical quality of source images. As this technique is preferably performed on contrast-enhanced images, this may further limit its applicability.

Diagnostic Performance

Diagnostic accuracy of texture analysis is highly variable, depending on the parameter or combination of parameters

being assessed as well as the type of image. On MRI, one study[56] found accuracies ranging from 0.67 for the detection of fibrosis stage ≥ 2 to 0.94 for the detection of cirrhosis. Another study[55] used several parameters and imaging sequences for their analysis and found the highest AUC to be 0.98 for separation of fibrosis stage ≤ 2 from fibrosis stage ≥ 3 on double contrast-enhanced images analyzed with a combination of two texture parameters.

Mechanical Changes in Liver Fibrosis

Liver fibrosis induces mechanical changes to the liver that are perceived qualitatively as increased stiffness by physical examination.[59] To complement the physical examination and provide quantitative assessment of mechanical properties, elastography methods were proposed to measure the shear wave propagation in the tissue, from which the shear wave speed (in m/s), the shear wave attenuation (in Np/m), the complex shear modulus (in Pa), the elasticity (in Pa), or Young's modulus (in Pa) could be reported. The physical parameter quantified in dynamic elastography is usually the shear wave speed. Assuming a model, mechanical parameters can then be approximated. The complex shear modulus G* corresponds to the resistance of a material to shear stress and has two components, the storage modulus G′ and the loss modulus G″. The storage modulus is the real part of G* and reflects the elastic component of the tissue. The loss modulus is the imaginary part of G* and represents the viscous component. G* can also be defined as the slope of the shear strain to shear stress relationship. Elasticity is a property of a material that tends to return to its original shape after deformation. The Young's modulus corresponds to the slope of the uniaxial strain–stress relationship that is equal to three times the shear modulus for isotropic and incompressible materials. Alternatively, mainly with MR-based methods, liver fibrosis could be studied with strain imaging approaches. Strain represents the deformation expressed in percent of the original segment length.

Liver fibrosis has an effect on all these tissue properties. Increases in fibrosis stage are associated with an exponential increase in liver stiffness and a corresponding increase in most listed properties (ie, shear wave speed, Young's modulus, G*, G′, and G″).[60–63] However, mechanical properties do not solely depend on the fibrosis stage, but also depend on technical and biological confounders. Technical confounders include the frequency of the applied shear wave, because of the dispersive behavior of tissues,[64,65] the depth of measurement,[66] and device dependencies. Biological confounders of tissue stiffness measurements include inflammation,[67] breathing motion,[68] and fasting or postprandial state of the patient.[69,70]

Elastography

Elastography techniques may be classified according to the type of deformation, source of deformation, timing of mechanical deformation, imaging modality on which they are implemented, and the volume assessed. The type of deformation is either produced by shear waves, as introduced earlier, or by a compression of the tissue (known as strain elastography). The source of deformation can be intrinsic and produced by physiological cardiac and respiratory motions; external, using a manual compression or a vibrator; or in situ with a radiation pressure inducing shear-waves, as in US shear wave elastography. Dynamic mechanical vibrations may be transient (very short duration, <30 msec) or harmonic (periodic motion applied throughout the image acquisition). The imaging modality is either US or MRI. Finally, the studied volume is either unidirectional (1D transient elastography), small (focal point radiation pressure), planar (US shear-wave elastography), multiple slices (2D MR elastography [MRE]), or large that may encompass the entire liver (3D MRE). There are therefore numerous existing elastography implementations.

In this article, we focus on shear-wave elastography techniques, which have found more applications in the diagnosis and staging of liver fibrosis. We also briefly comment on MRI strain imaging, which is distinct from MRE. A classification of elastography techniques is shown in Fig. 3. Illustrations of shear elastography techniques and companion examples are provided in Fig. 4.

US Shear-Wave Elastography
Concept
Shear wave elastography techniques measure the propagation speed and amplitude decay of mechanical shear waves inside the tissue. Most imaging methods, however, simply rely on the shear wave speed, which increases with higher fibrosis stages.

Numerous US-based shear wave elastography techniques have been described.[71] Of these, three are most widely used clinically and are succinctly described: 1D transient elastography, focal point shear-wave elastography, and supersonic shear-wave elastography. With US, excitation frequencies typically range from 50–400 Hz. Since mechanical properties are frequency-dependent and elastographic techniques use different excitation frequencies and report their results in different units, the thresholds for staging liver fibrosis cannot be directly compared.

In 1D transient elastography, commercialized as Fibro-Scan (Echosens, Paris, France), a piston-mounted transducer induces a mechanical vibration of 50 Hz at the surface of the skin above the liver. The resulting shear waves are tracked to measure their propagation speed, which is converted to a Young's modulus.[72]
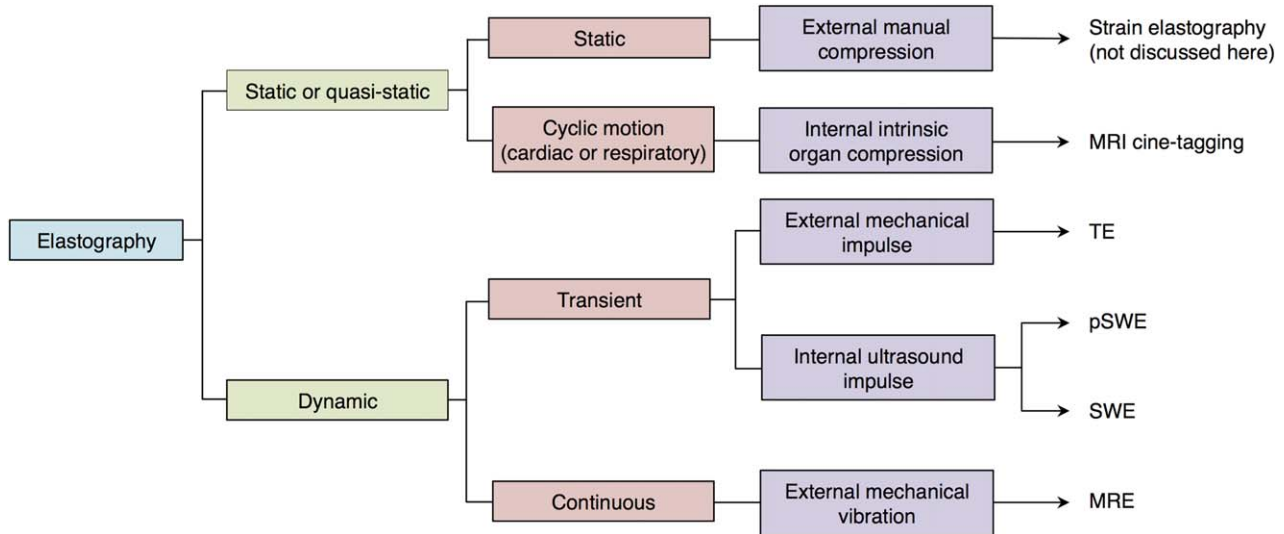
FIGURE 3: Classification of US-based and MR-based elastography techniques. TE = transient elastography. pSWE = point shear wave elastography. SWE = shear wave elastography. MRE = magnetic resonance elastography.

To perform focal point shear-wave elastography, commercialized as ARFI (acoustic radiation force impulse, Siemens Medical Solutions, Mountain View, CA), a radiation pressure is created and focused on one point at a time in the tissue. The acoustic energy from the impulse is converted to mechanical shear waves. These are mapped in 2D using US tracking pulses, and the resulting tissue displacement is measured.[73] New implementation of this method relies on multiple focal points and assessment of the shear wave speed.

Supersonic shear-wave elastography, commercialized by Supersonic Imagine (Aix-en-Provence, France), uses multiple spherical wave fronts, which are created at increasing depths in the tissue at a speed faster than that of the shear waves, thus producing a Mach cone. The propagation of this shear wave cone is then imaged at an ultrahigh frame rate ($\sim$15,000 Hz) in the entire imaging field of view to capture shear wave speeds. This allows the real-time generation of elastograms representing the Young's modulus of the tissue
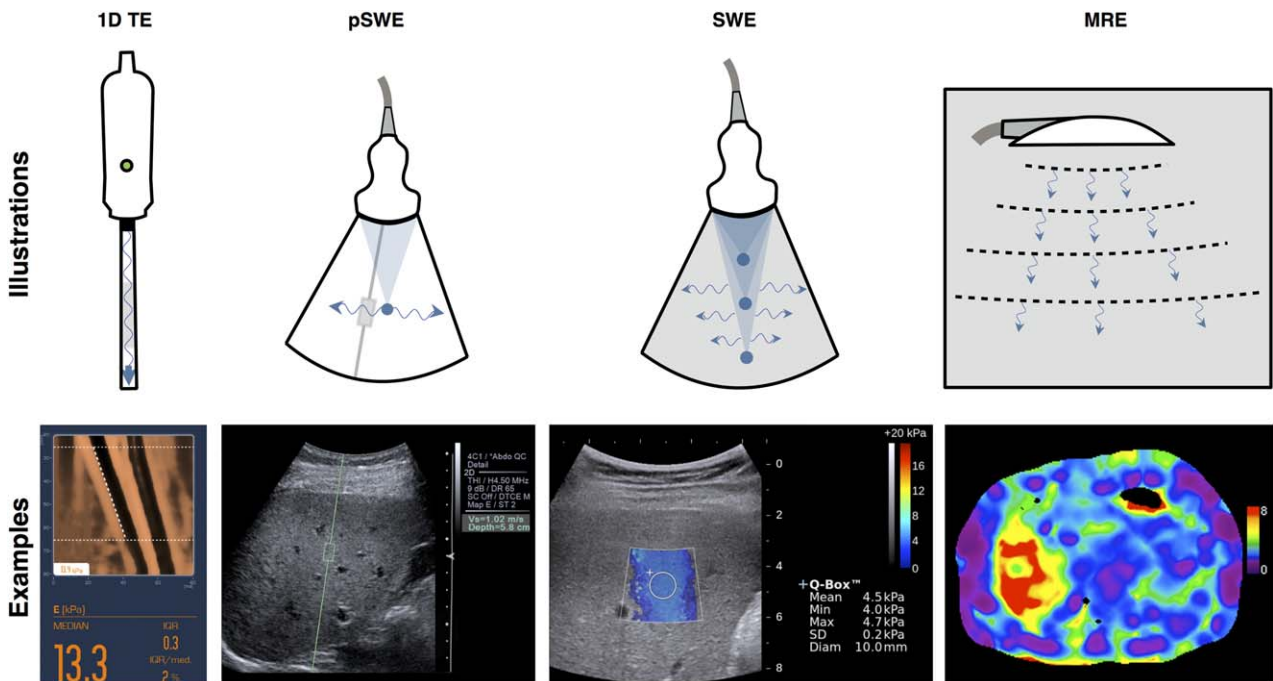
FIGURE 4: First row: illustrations of probes used by each shear elastography techniques with field of view (black outline), source and direction of shear wave propagation (blue arrows), and regions of interest (gray surfaces). Second row: companion images that illustrate 1D transient elastography (TE), point shear wave elastography (pSWE), shear wave elastography (SWE), and magnetic resonance elastography (MRE). Transient elastography image courtesy of Laurent Sandrin (Echosens, Paris, France).
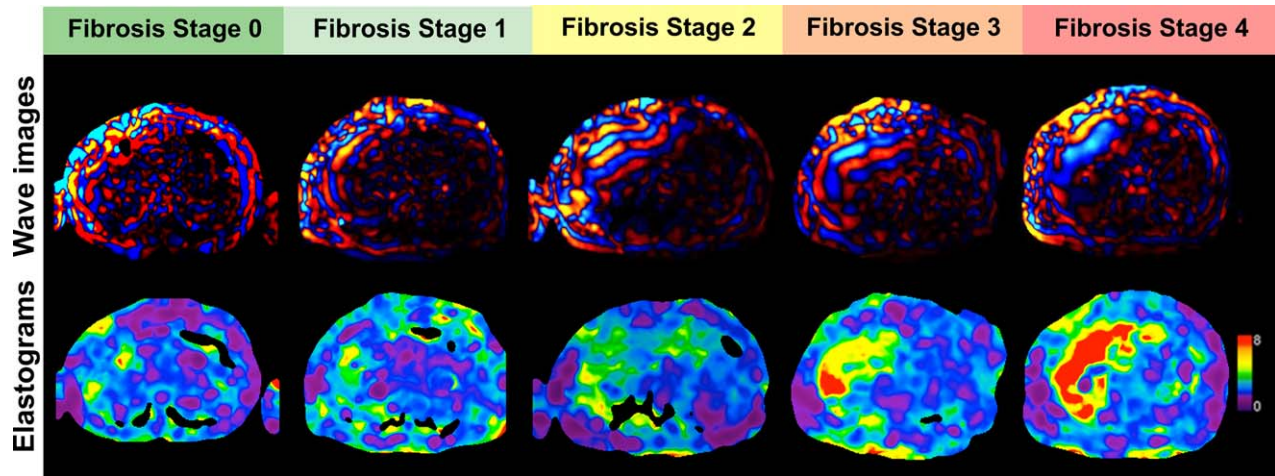
FIGURE 5: MRE in five different patients with fibrosis stages 0 to 4 confirmed by liver biopsy. Top row shows axial wave images and bottom row shows corresponding axial stiffness maps (also known as elastograms) with a scale from 0 to 8 kPa.

(depending on regulation approval, either the shear wave speed or Young's modulus map is provided).[74]

Advantages and Limitations

US elastography techniques are portable, relatively inexpensive, fast to acquire, and do not require postprocessing.[75] In particular, 1D transient elastography has been widely validated in clinical trials, adopted clinically, and used by clinicians at point of service.

However, US elastography techniques may be technically inadequate in obese patients or those with a narrow intercostal space. Because of US attenuation, measurement of shear waves may be unreliable in deeper regions of the liver. Also, patients with ascites cannot be assessed with 1D transient elastography because shear waves cannot propagate in a liquid medium, although this is seldom a clinical concern because these patients usually have known cirrhosis.[76] The region of interest (ROI) is smaller with US elastography than MRE techniques. Further, US elastography implementations are not yet standardized, thus preventing application of shear wave speed thresholds obtained from different manufacturers.

Diagnostic Performance

The diagnostic accuracy of US elastography techniques has been assessed in numerous studies and pooled in meta-analyses for 1D transient elastography[77–80] and focal point shear-wave elastography.[80,81] This validation was performed in an era when liver biopsy was still an acceptable clinical reference standard for confirmation of liver fibrosis stage.

The reported diagnostic accuracy is similar for various US elastography techniques, with an AUC in the range of 0.84–0.87 for fibrosis stage ≥ 2, 0.89–0.91 for fibrosis stage ≥ 3, and 0.93–0.96 for fibrosis stage 4. Hence, the diagnostic accuracy tends to increase from significant (stage 2) to advanced fibrosis (stage 3) and cirrhosis (stage 4).

MR Elastography

Concept

MRE is a dynamic technique to measure shear wave propagation. The general concept is that shear wavelength (and hence shear wave speed) is related to tissue stiffness. Examples of MRE shear wave images and stiffness maps in patients with fibrosis stages from 0 to 4 are provided in Fig. 5.

MRE requires three components: 1) a driver to generate mechanical waves; 2) a phase-contrast pulse sequence with motion-encoding gradients (MEG) to detect tissue motion, obtain information on wave motion and magnitude MR images to view anatomy, and generate cine wave images; and 3) postprocessing to obtain wave images and inversion algorithms to produce quantitative maps of mechanical properties (also known as elastograms).

DRIVER. Several types of drivers have been developed for the creation of mechanical waves in MRE. These can be classified according to the location of the actuator.[82] The most widely used design relies on an active driver located in the equipment room that creates air pressure waves transmitted through a plastic tube to a passive driver placed against the patient's abdominal wall adjacent to the liver. This design has been commercialized by Resoundant (Rochester, MN) and licensed to major MRI manufacturers.

Drivers can induce shear waves directly at the skin surface or compression waves that are then converted to shear waves by a process known as mode conversion. Compression waves have better penetration and travel more rapidly than shear waves and the displacement information due to these waves can be filtered out during postprocessing.[83]

The induced vibrations are either at a single frequency (eg, 60 Hz[63]) or multiple frequencies.[83] Typical excitation frequencies of MR elastography range from 40–80 Hz for liver imaging.[63,64,84]

PULSE SEQUENCE. The induced shear waves are then imaged with a phase-contrast MR pulse sequence. This MRE concept has been implemented on several different types of sequences, including spin-echo,[85] gradient-recalled echo,[86] echo-planar imaging,[64] and balanced steady-state free-precession.[87] Motion-encoding gradients synchronized with the excitation waves are used to detect small displacements in the range of tens of microns in the encoding direction.[88] Both sinusoidal and trapezoidal gradient shapes have been investigated for this use.[89] Typical gradients have a temporal length of one period of the applied vibration, but shorter gradients (eg, higher harmonics of the wave) have also been employed to reduce the length of the image acquisition.[87,90] The movements of the tissue are thus encoded into the resulting signal, in which the phase is proportional to the amplitude of the wave.

IMAGE ACQUISITION. Acquired images include phase and magnitude information. The phase images reveal the shear wave propagation data, ie, the shear wave length and amplitude decay. The magnitude images contain the anatomical information, which is subsequently used to identify regions of interest in the liver to exclude the liver capsule and major vessels.

MULTIPHASE ACQUISITION. Unlike US elastography, which relies on ultrafast imaging to track shear wave motion, MRE applies dynamic (ie, cyclical) shear waves that are imaged using stroboscopic snapshots of wave motion to create cine wave images. This is achieved by repeating the MR image acquisition with different phase offsets between the motion-encoding gradients and the mechanical wave induced in the tissue.

POSTPROCESSING. Phase images can be directly converted to so-called wave images, which reveal both the amplitude and wavelength of shear waves in the tissue. A curl operator is applied to eliminate the unwanted compression wave component of the image and to isolate the shear waves. Then an inversion algorithm is used to extract a quantitative map of the mechanical properties of the liver (also known as "elastogram"). In clinical practice, this elastogram usually represents the magnitude of the complex shear modulus $|G|$, although quantitative maps of storage modulus (G') or loss modulus (G'') are commonly reported in a research setting. Several inversion algorithms have been implemented, relying on different assumptions about the geometry, homogeneity, isotropy or anisotropy, and viscoelasticity of the liver tissue.[88,91]

MEASUREMENT. From the elastograms, measurements of tissue mechanical properties can be made. One typically selects an ROI in the liver parenchyma while avoiding major vessels and the liver capsule. A recent study[92] has proposed an algorithm for automatic artifact correction and segmentation using information from MRE magnitude images. Of note, the resulting mechanical properties do not depend on the magnetic field strength of the MR system.[93]

Advantages and Limitations

Unlike US elastography, the commercially available MRE technique has been standardized across major MR manufacturers. MRE is a reliable technique for assessing liver stiffness, with little variability between MR manufacturers, field strengths, and pulse sequences.[94,95] Pooled data from meta-analyses of elastography techniques show that MRE provides higher diagnostic accuracy for staging liver fibrosis than 1D US transient elastography, focal point shear-wave US elastography, and MR diffusion-weighted imaging. However, the majority of studies from which these meta-analyses are based have not performed head-to-head comparison of MRE with other techniques.[96–98] Nevertheless, the few studies that have done so have reported higher diagnostic performance for MRE than 1D transient elastography[99] and supersonic shear-wave elastography.[100] MRE has higher diagnostic accuracy for staging of all fibrosis stages.[101]

It is a robust technique, which allows measurements in larger patients or even those with ascites.[102] Further, it typically covers a larger liver volume than US elastography techniques, which may reduce sampling variability. However, the biological confounding factors applying to US elastography techniques (such as postprandial state; concomitant liver steatosis, inflammation, cholestasis; right heart failure and hepatic venous congestion) also apply to MRE. Current MRE sequences are sensitive to liver iron overload, which lowers the signal-to-noise ratio in the parenchyma and may lead to unreliable measurements or technical failure.[103] This limitation is especially prevalent at higher field strength (ie, 3.0T) and when using a gradient-echo-based sequence. MR-based elastography is also more prone to motion artifacts than US elastography. Current MRE implementations rely on image postprocessing before the results can be appreciated. Automated algorithms for ROI placement, however, are in development.[92] Finally, MRE requires additional hardware to be added to the MR scanner, although the incremental cost is lower than that of US-based elastography techniques.[59]

Diagnostic Performance

The diagnostic accuracy of MRE has been assessed using liver biopsy as the reference standard. Four meta-analyses of the diagnostic performance of MRE are available,[96–98,104] which cover 19 studies and a cumulative total of 1441 patients. MRE provides higher overall diagnostic accuracy than US-based elastography. These meta-analyses report AUC in the range of 0.84–0.95 for diagnosing fibrosis stage ≥ 1, 0.88–0.98 for fibrosis stage ≥ 2, 0.93–0.98 for fibrosis stage ≥ 3, and 0.92–0.99 for fibrosis stage 4. Hence, similar
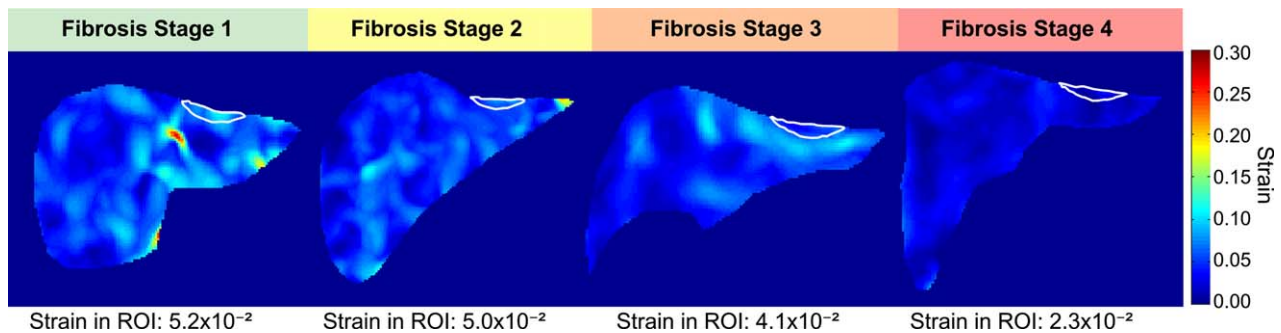
FIGURE 6: Strain maps of patients with fibrosis stages 1 to 4 confirmed by liver biopsy. Note that strain values in ROI decrease with increasing fibrosis stages.

to US elastography techniques, the diagnostic accuracy of MRE tends to increase from lower to higher fibrosis stages.

MR Strain Imaging

Concept
MR strain imaging measures the liver deformation in response to physiological motion (either cardiac or respiratory).[105] Liver strain is high in normal liver and lower in cirrhotic liver. Examples of strain maps in patients with fibrosis stages from 1 to 4 are shown in Fig. 6.

MR strain imaging can refer to two technical variants: cine-tagging or strain-encoded imaging. In cine-tagging, the underlying MR image is modulated by a magnetization grid that moves with the tissue. This grid is generally created using the spatial modulation of magnetization sequence (SPAMM) or one of its variants (eg, CSPAMM); however, other methods are also available for tagging (eg, DANTE). Several phases are acquired in the cardiac cycle. The resulting 2D grid or "tags" allow the tracking of tissue movement created by cardiac motion.[106,107] Several analysis methods are available to convert these images to strain maps, the most widely used being the harmonic phase (HARP) analysis method. They usually rely on the isolation of harmonic peaks of the image in the Fourier space to extract phase information from which tag positions can be extracted. The final step is to select an ROI for measuring representative strain for each patient.[108,109] Alternatively, strain-encoded imaging gives a direct measurement of strain through a similar process that encodes strain into the signal by varying the spatial frequency of artificial tags in the image.[110]

Advantages and Limitations
Cine-tagging and strain-encoded imaging have the advantage of requiring no additional hardware and can be done on any clinical MR system without the need for a contrast agent. They also allow measurement of strain in the left lobe of the liver, which may be more difficult to assess using other techniques such as diffusion-weighted imaging and MRE because the transducer is typically placed above the right liver. However, postprocessing is required for strain calculation and placement of the ROI.

Diagnostic Performance
The diagnostic performance of MR strain imaging has not been assessed for staging fibrosis in its early stages. Studies have focused on differentiation between normal and cirrhotic livers[109,110] or compared liver strain in patients with cirrhosis with different Child–Pugh scores.[108] The reported diagnostic accuracy of cine-tagging for classification of Child–Pugh A or greater is in the range of 0.910–0.998 and for Child–Pugh B or greater in the range of 0.806–0.934. Additional studies are required to evaluate the diagnostic accuracy of strain imaging for the staging of liver fibrosis.

$T_1\rho$

Concept
The spin-lattice relaxation time in the rotating frame, or $T_1\rho$, increases with higher fibrosis stages.

$T_1\rho$ refers to a phenomenon that occurs when tipping the magnetization of spins into the transverse plane before applying a radiofrequency pulse that creates a spin-lock state, leading to a low-frequency precession (typically 500 Hz).[111] The relaxation time of this transverse magnetization is known as $T_1\rho$.[112] The application of a radiofrequency field (B_1) to the volume creates an effective field, B_{eff}, which rotates around B_0 at a certain angle and at the Larmor frequency. In the rotating reference frame, the magnetization of the spins is first oriented parallel to B_{eff}, then tipped by the desired flip angle by applying a pulse whose length is defined as the spin-lock time. To measure this, several spin-lock times are required to sample the monoexponential decay of transverse magnetization.[113] Examples of $T_1\rho$-weighted images for the calculation of a $T_1\rho$ map are provided in Fig. 7.

Because of the low frequency of precession, $T_1\rho$ is sensitive to low-frequency motion of molecules and static processes, making it a good indicator of the presence of macromolecules, such as the proteins that accumulate in the liver as a consequence of fibrosis.[112] $T_1\rho$ has been found to increase in cirrhotic livers[114] and some studies have found it to correlate with fibrosis stage.[115,116] The mechanisms
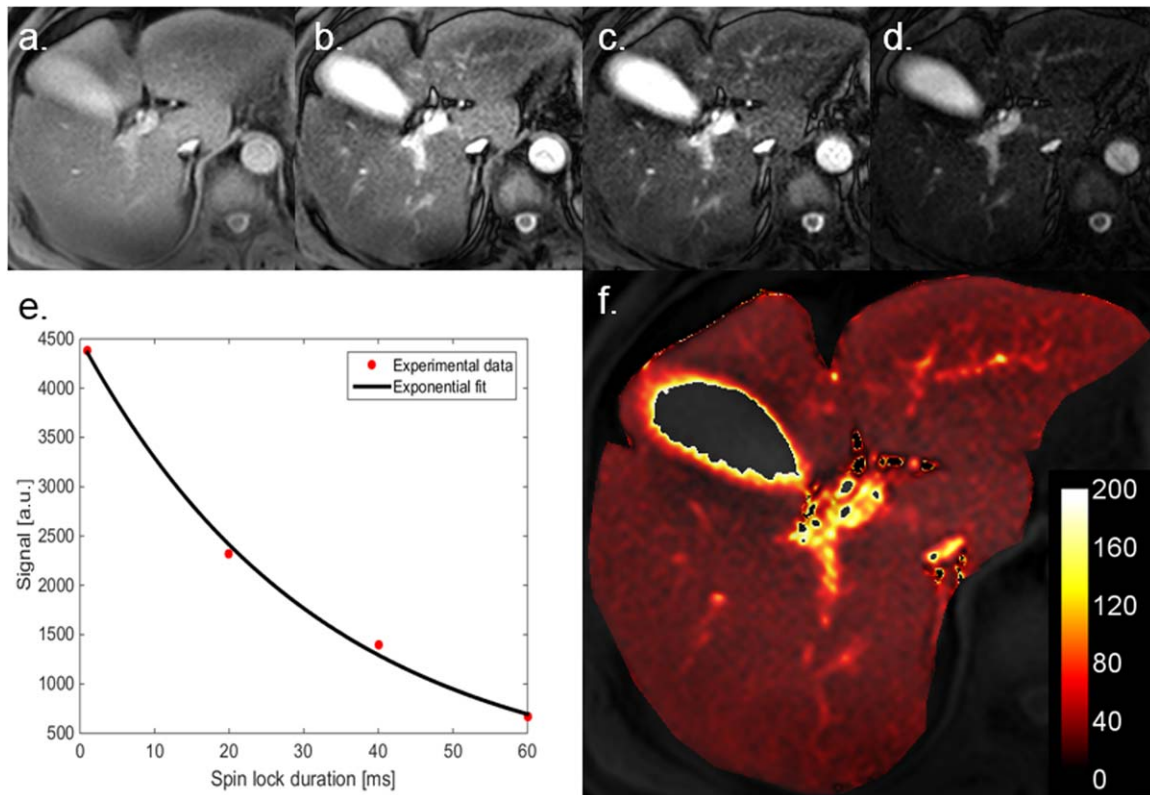
FIGURE 7: $T_1\rho$-weighted images with spin lock durations of (a) 1 msec, (b) 20 msec, (c) 40 msec, and (d) 60 msec. e) Typical signal decay as a function of the spin lock duration in the liver parenchyma. f) $T_1\rho$ map (msec).

underlying the change in $T_1\rho$ in fibrotic disease are not yet known, and collagen deposition may not be the only factor affecting this parameter.

Advantages and Limitations

$T_1\rho$ quantification has the advantage of being unaffected by the postprandial or fasting state of the patient.[117] It also requires no contrast agent or additional hardware, and appears not to correlate with the degree of steatosis or the iron load of the liver, although reported results are based on a limited sample size.[114]

However, this technique typically has increased sensitivity to B_0 and B_1 field inhomogeneities and is associated with higher specific absorption rate,[118] which can lead to technical complications at higher field strength.

Diagnostic Performance

The diagnostic performance of the $T_1\rho$ quantification technique for staging of liver fibrosis has been assessed in a few recent studies that have used histopathology as the reference standard. The AUC was 0.97 for differentiation of normal (stage 0) from cirrhotic (stage 4) liver in a preliminary study.[114] Another study found a significant differentiation ($P = 0007$) between normal and cirrhotic livers.[119] For staging of liver fibrosis, early studies provide contradictory results. Although a clinical study has shown significant increases of $T_1\rho$ with higher fibrosis stage, without reporting

corresponding AUCs,[115] a larger study has found no correlation between fibrosis stage and $T_1\rho$ values.[120] Additional results are required to assess the diagnostic accuracy of $T_1\rho$ for staging of liver fibrosis and to compare this technique with MRE.

Diffusion-Weighted Imaging

Concept

Diffusion-weighted imaging (DWI) provides information on the Brownian motion of water molecules in each imaging voxel. Diffusion is restricted with higher fibrosis stages. Examples of apparent diffusion coefficient maps in patients with fibrosis stages from 0 to 4 are provided in Fig. 8.

Diffusion of water molecules is typically measured by applying a pair of bipolar gradients that successively dephases and rephases the spins of the volume. The phase dispersion is related to motion of water molecules along the gradient direction. The gradients applied are characterized by the b-factor, with units of s/mm^2. Molecules moving during the time between the gradients contribute to diminishing the magnitude signal of the image, as a result of intravoxel dephasing.

Two models are most frequently applied to fit the data: the monoexponential model or the biexponential model. The monoexponential model requires a minimum of two b-values (in general 0 s/mm^2 and a high b-value, ≥ 200 s/mm^2) to fit a linear equation to the semilogarithmic
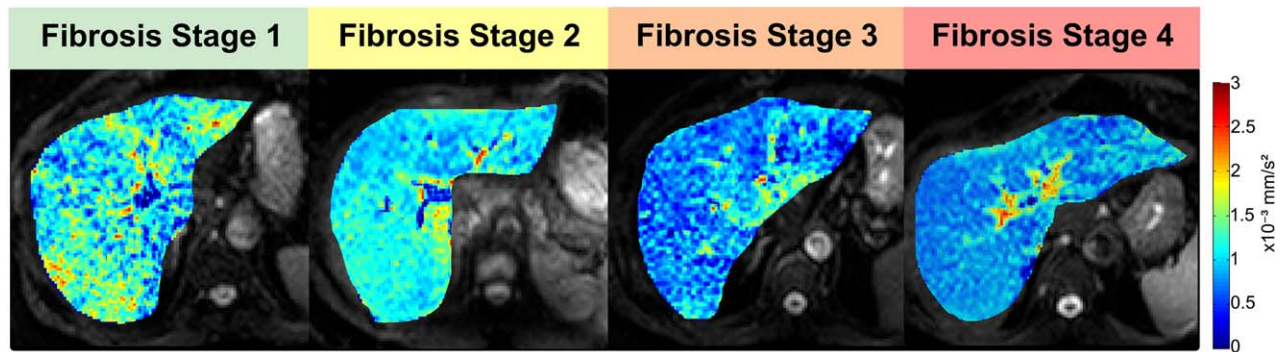
ADC in ROI = 1.2 x 10⁻³ ADC in ROI = 1.1 x 10⁻³ ADC in ROI = 8.4 x 10⁻⁴ ADC in ROI = 8.1 x 10⁻⁴

FIGURE 8: ADC maps of patients with fibrosis stages 0 to 4 confirmed by liver biopsy. Note that ADC values decrease with increasing fibrosis stages.

plot.[121] This gives a measurement of the apparent diffusion coefficient, or ADC, which grows with an increase in diffusion. The biexponential model is used in a method known as intravoxel incoherent motion (IVIM).[122] To acquire diffusion parameters according to the IVIM model, several diffusion-weighted images at different b-values, including a large number of small b-values, must be acquired. Capillary perfusion can be estimated from low b-values (<200 sec/mm^2) and molecular diffusion from high b-values (≥ 200 s/mm^2). Three parameters are extracted from the IVIM model: the perfusion fraction (f) and two components contributing to signal loss: diffusion (D) and perfusion (D^*), often referred to as pseudo-diffusion.[123]

There are conflicting results as to the relationship between the ADC and fibrosis stage. Some studies have shown a decrease in ADC with increasing fibrosis stage, which may be explained by the presence of collagen fibers restricting molecular motion.[124–128] One study[129] showed that ADC decreased with fibrosis stage in living rats, but not in dead rats, suggesting that perfusion may be a more important factor in the decrease of ADC than molecular diffusion. On the other hand, studies have shown a significant decrease in D^*,[130–134] D[131–134] (other studies did not observe this decrease in D). and f[132–134] (other studies found f to be unchanged). D^*, which is related to perfusion rather than diffusion, shows the most drastic decrease of these parameters. The decrease in perfusion is explained by the presence of collagen deposits and stellate cells that increase the resistance to blood flow in the liver and contribute to portal hypertension.[135]

Advantages and Limitations

DWI is available on most MR scanners and does not require specialized hardware. Its acquisition is relatively fast and does not require contrast injection, which explains its clinical adoption in liver imaging.

However, there are several limitations to this technique. First, the b-values used from one center to the other are not standardized, and it has been shown that b-value

does have an impact on measured ADC.[136,137] Therefore, ADC values cannot be compared from one study to the other and cutoff values for staging liver fibrosis are difficult to establish. ADC is also sensitive to image noise, which makes comparison between vendors and scanners more difficult. Additionally, diffusion-weighted MRI is intrinsically affected by motion, which makes measurements unreliable in the left lobe of the liver due to cardiac motion. Confounding factors of DWI include incomplete fat saturation and iron deposition in the liver.[138]

Diagnostic Performance

The diagnostic accuracy of DWI has been assessed using liver biopsy as the reference standard. A meta-analysis of DWI studies assessing monoexponential analysis of ADC for the staging of liver fibrosis included 10 studies with a cumulative total of 613 patients.[96] This meta-analysis reported AUC of 0.86 for fibrosis stage ≥ 1, 0.83 for fibrosis stage ≥ 2, and 0.86 for fibrosis stage ≥ 3.

More recently, some studies have examined IVIM for staging of liver fibrosis. A study has found that D^* was more accurate in determining the stage of fibrosis than ADC.[134]

However, a combination of the three parameters extracted from IVIM may provide higher diagnostic accuracy than ADC alone.[132] Standardization of the IVIM technique is required before thresholds may be adopted clinically.

Perfusion

Concept

In perfusion imaging, liver signal enhancement after injection of contrast agents is used to assess liver function. Changes in semiquantitative or quantitative parameters may be related to liver fibrosis stages. Examples of dynamic contrast-enhanced images and corresponding signal intensity curves are shown in Fig. 9.

Perfusion imaging has been performed with US, CT, and MRI, but this review will focus on MRI-based
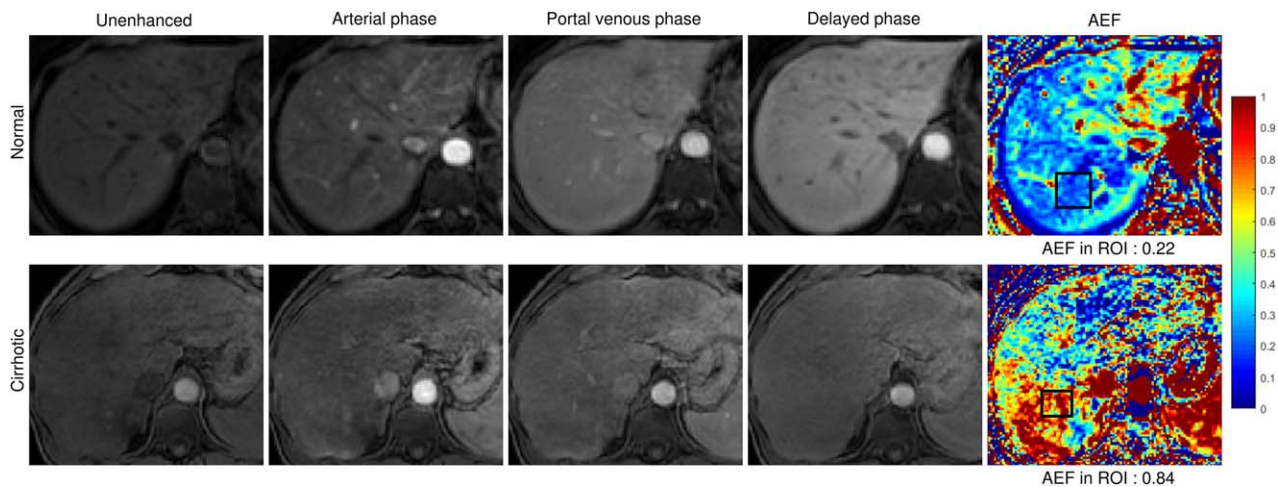
FIGURE 9: T_1-weighted fat-saturated MRI before and after injection of extracellular gadolinium contrast agent in normal (top row) and cirrhotic (bottom row) patients. Note that arterial enhancement fraction (AEF) values are higher in cirrhosis.

perfusion. MRI typically uses gadolinium-based contrast agents, which increase the signal of blood in a T_1-weighted sequence by decreasing its T_1 relaxation time. Signal intensity is typically measured in the abdominal aorta as a surrogate for the hepatic artery, the portal vein, and the liver parenchyma.[139] Model-free analysis of the enhancement curves results in semiquantitative parameters such as time to peak, peak concentration, and upslope.[133,140,141]

For quantitative imaging, signal intensity is converted to contrast agent concentration, first by calculating the T_1 of each region using either a linear or nonlinear relationship,[142] then by assuming a linear relationship between R1 ($1/T_1$) and concentration of gadolinium. Various pharmacokinetic models are used to extract more quantitative perfusion parameters. Several models have been proposed for the analysis of perfusion data,[140] and they differ in the number of feeding vessels and tissue compartments. In the liver, the dual-input single compartment model is most often used to account for the dual vascular supply of the hepatic artery and portal vein. Two-compartment (intravascular and extravascular extracellular space) and three-compartment models (intravascular, extravascular extracellular space, and hepatocellular space) have been assessed. Parameters measured with these techniques include arterial and portal fractions as well as mean transit time of contrast agent. Others have measured the arterial enhancement fraction, which is represented by (arterial phase signal intensity minus the unenhanced intensity) divided by (portal phase signal intensity minus the unenhanced intensity).[143,144] Portal fraction has been shown to decrease[133,145] and arterial enhancement fraction to increase[143,144] with increasing fibrosis stage.

Advantages and Limitations

This concept has the advantage of being applicable to any contrast-enhanced imaging modality (CEUS, dynamic contrast-enhanced [DCE]-CT and DCE-MRI) and has

potential for prognostic significance, as perfusion parameters could be used to predict treatment outcome. However, patient cooperation is essential for intravenous injection of a contrast agent. Postprocessing of perfusion images is potentially lengthy, and the analysis is not standardized from one center to the other due to the use of different models and assumptions.

Diagnostic Performance

Using the arterial enhancement fraction for the staging of fibrosis, one study found AUCs of 0.83 for fibrosis stage ≥1, 0.85 for fibrosis stage ≥2, 0.88 for fibrosis stage ≥3, and 0.92 for fibrosis stage 4.[143] The diagnostic performance of perfusion imaging for the staging of fibrosis therefore increases with higher fibrosis stage.

Hepatocellular Function

Concept

The uptake of hepatobiliary contrast agents may be used as a surrogate marker of liver function, which decreases with higher fibrosis stages. Examples of ΔR1-based hepatocyte fraction maps showing the uptake of a hepatobiliary contrast agent are shown in Fig. 10.

Two hepatobiliary contrast agents are available, gadoxetate disodium and gadobenate dimeglumine, whose uptake depends on the expression of transporters, related to function of hepatocytes.[146] These can be used to assess liver function by acquiring images before contrast injection and in hepatobiliary phase of uptake (20 min after gadoxetate disodium injection). Different measurements of hepatic function can be used, such as relative enhancement compared to precontrast signal,[147–149] relative signal intensity compared with other organs (such as the spleen, muscles, or spinal cord),[150,151] or both.[152] Because fibrosis impedes hepatic function, contrast enhancement tends to diminish with increasing fibrosis stage. Recently, other studies have
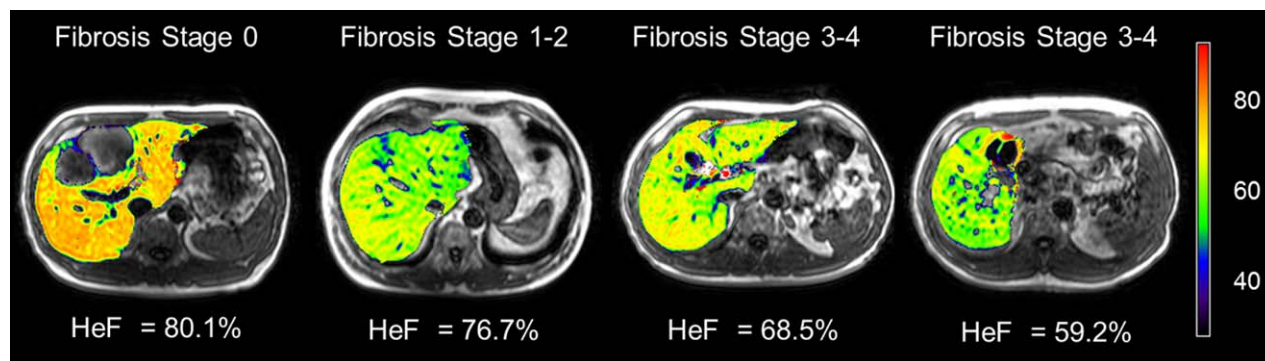
FIGURE 10: Hepatocyte fraction (HeF) maps in four different patients with various fibrosis stages. Note that the hepatic uptake of gadoxetate disodium decreases with higer fibrosis stages. Image courtesy of Tomoyuki Okuaki (Philips Healthcare, Tokyo, Japan).

employed different approaches for the measurement of liver function. One of them[153] used the signal enhancement curve of the liver parenchyma to extract semiquantitative parameters such as those measured in DCE-MRI. Others have used pharmacokinetic modeling and $\Delta R1$ to extract the hepatocyte fraction, which has shown a negative correlation with fibrosis stage.[154,155]

Advantages and Limitations

Evaluation of hepatobiliary function can be done on any clinical MRI system, and is already a routine examination for liver fibrosis in some centers. Postprocessing of the images is simple and fast.

However, this technique requires injection of hepatobiliary contrast agents, which are more costly than extracellular agents, and requires at least a 20-minute delay for hepatobiliary phase imaging, which lengthens the examination.

Diagnostic Performance

Diagnostic performance varies from one study to the other and depends on the parameters being assessed. Studies found AUCs of 0.63,[151] 0.85,[149] 0.87,[150] and 0.93[152] for detection of fibrosis stage ≥ 3. The detection of other fibrosis stages has not been assessed. More studies are warranted with a uniformized protocol and analysis method for better evaluation of diagnostic performance.

Miscellaneous

Additional MRI contrast mechanisms have been investigated for the staging of liver fibrosis. T_1 mapping on hepatobiliary contrast-enhanced images[156,157] shows an increase in liver T_1 in fibrotic or cirrhotic livers. Susceptibility-weighted imaging[158,159] shows a decrease in liver-to-muscle signal intensity ratio that correlated with fibrosis stage. Recently, a new contrast agent targeting collagen, EP-3533, has been created for molecular imaging of fibrosis.[160] This agent has been tested in rats but human studies have yet to be conducted.[161–163]

Future Directions

Imaging techniques address an important limitation of liver biopsy: their noninvasive nature eliminates the risk of hemorrhagic complications and improves acceptability for patients and physicians. Yet, despite this large array of imaging techniques to evaluate liver fibrosis noninvasively, there are still some clinical needs that are not completely addressed.

Because of its inherently volumetric nature, MRI encompasses the entire liver volume. This may help resolve the sampling variability that affects US elastography techniques that sample a small liver volume. However, the current 2D MRE technique available commercially evaluates liver stiffness in four slices. Recently, the introduced 3D MRE technique shows promise for assessment of the entire liver volume.[164] MRE is a highly accurate technique for the staging of liver fibrosis, but it is affected by a technical failure rate of 5.6%, especially in patients with iron deposition.[102] Investigational sequences may improve coverage, robustness to iron deposition, and technical success.[164,165]

To facilitate clinical adoption and to minimize the variability between MRI manufacturers and field strengths, there is a need to standardize acquisition techniques (other than MRE, which is already well standardized between vendors and centers)—including pulse sequence parameters—and postprocessing. In turn, this will permit application of thresholds obtained from different MRI scanners.

The inclusion of MRI sequences for assessment of liver fibrosis adds MRI acquisition time. Sequences that simultaneously assess different contrast mechanisms may help reduce total acquisition time while providing multiparametric imaging.[166]

Another barrier to clinical adoption is the requirement for time-consuming postprocessing with most current MR-based quantitative techniques. Automation and faster calculation of quantitative parameters will be required for real-time interpretation by the radiologist. The inclusion of automated liver segmentation, which alleviates the need for

ROI placement by users, will also reduce interobserver variability.

Chronic liver diseases are characterized by the presence of liver fibrosis, fat, inflammation, biliary disease, and iron. The concomitant presence of these pathological changes may act as confounders to liver fibrosis staging. Multiparametric techniques are required to assess and control for the effect of these biological confounders on the diagnosis and staging of liver fibrosis. In particular, quantification of liver steatosis may be helpful for the management and monitoring of NASH patients.[14] While preliminary results suggest that MRE may detect inflammation, a marker of activity grade, future clinical studies are required to validate this concept.[167,168] Finally, recent studies suggest that combining parameters yields better diagnostic performance than single parameters for staging of liver fibrosis.[133,159,169]

Conclusion

In summary, qualitative and quantitative imaging techniques for the staging of liver fibrosis have been implemented on US, CT, and MRI scanners to address the limitations of liver biopsy. These imaging techniques assess changes in morphology or physical properties such as texture, mechanical properties, $T_1\rho$, diffusion, perfusion, and hepatocellular function. Among these techniques, US elastography is the most widely used clinically. However, MRE has higher diagnostic accuracy for staging liver fibrosis than US elastography and other MR-based techniques. Further, MRI has the potential for comprehensive assessment of the pathological changes usually observed using liver biopsy. In the future, a "one-stop-shop" multiparametric protocol may leverage the numerous tissue contrast mechanisms of MRI for simultaneous assessment of liver fibrosis as well as inflammation, biliary disease, fat, and iron deposition.

Acknowledgments

References

1. Bataller R, Brenner D. Liver fibrosis. J Clin Invest 2005;115:209–218.

2. Kim WR, Brown RS, Terrault NA, El-Serag H. Burden of liver disease in the United States: Summary of a workshop. Hepatology 2002;36: 227–242.

3. Bedossa P, Carrat F. Liver biopsy: The best, not the gold standard. J Hepatol 2009;50:1–3.

4. Rockey DC, Caldwell SH, Goodman ZD, Nelson RC, Smith AD. Liver biopsy. Hepatology 2009;49:1017–1044.

5. Sebastiani G, Gkouvatsos K, Pantopoulos K. Chronic hepatitis C and liver fibrosis. World J Gastroenterol 2014;20:11033–11053.

6. Lee UE, Friedman SL. Mechanisms of hepatic fibrogenesis. Best Pract Res Clin Gastroenterol 2011;25:195–206.

7. Younossi Z, Koenig A, Abdelatif D, Fazel Y, Henry L, Wymer M. Global epidemiology of non-alcoholic fatty liver disease-meta-analytic assessment of prevalence, incidence and outcomes. Hepatology 2015;0.1–67.

8. Schuppan D, Afdhal NH. Liver cirrhosis. Lancet 2008;371:838–51.

9. Bedossa P, Bioulac-Sage P, Callard P, et al. Intraobserver and interobserver variations in liver biopsy interpretation in patients with chronic hepatitis C. Hepatology 1994;20:15–20.

10. Knodell RG, Ishak KG, Black WC, et al. Formulation and application of a numerical scoring system for assessing histological activity in asymptomatic chronic active hepatitis. Hepatology 1981;1:431–435.

11. Ishak KG. Chronic hepatitis: morphology and nomenclature. Mod Pathol 1994;7:690–713.

12. Brunt EM, Janney CG, Di Bisceglie AM, Neuschwander-Tetri BA, Bacon BR. Nonalcoholic steatohepatitis: A proposal for grading and staging the histological lesions. Am J Gastroenterol 1999;94:2467–2474.

13. Kim SU, Oh HJ, Wanless IR, Lee S, Han KH, Park YN. The Laennec staging system for histological sub-classification of cirrhosis is useful for stratification of prognosis in patients with liver cirrhosis. J Hepatol 2012;57:556–563.

14. Reeder SB, Cruite I, Hamilton G, Sirlin CB. Quantitative assessment of liver fat with magnetic resonance imaging and spectroscopy. J Magn Reson Imaging 2011;34:729–749.

15. Hernando D, Levin YS, Sirlin CB, Reeder SB. Quantification of liver iron with MRI: State of the art and remaining challenges. J Magn Reson Imaging 2014;40:1003–1021.

16. Maharaj B, Leary WP, Naran AD, et al. Sampling variability and its influence on the diagnostic yield of percutaneous needle biopsy of the liver. Lancet 1986;327:523–525.

17. Pagliaro L, Rinaldi F, Craxi A, Di Piazza S, Filippazzo G. Percutaneous blind biopsy versus laparoscopy with guided biopsy in diagnosis of cirrhosis. Dig Dis Sci 1983;28:39–43.

18. Regev A, Berho M, Jeffers LJ, et al. Sampling error and intraobserver variation in liver biopsy in patients with chronic HCV infection. Am J Gastroenterol 2002;97:2614–2618.

19. Colloredo G, Guido M, Sonzogni A, Leandro G. Impact of liver biopsy size on histological evaluation of chronic viral hepatitis: The smaller the sample, the milder the disease. J Hepatol 2003;39:239–244.

20. Afdhal NH, Nunes D. Evaluation of liver fibrosis: A concise review. Am J Gastroenterol 2004;99:1160–1174.

21. Hübscher SG. Histological grading and staging in chronic hepatitis: Clinical applications and problems. J Hepatol 1998;29:1015–1022.

22. Guido M, Rugge M. Liver biopsy sampling in chronic viral hepatitis. Semin Liver Dis 2004;24:89–97.

23. Bedossa P, Dargère D, Paradis V. Sampling variability of liver fibrosis in chronic hepatitis C. Hepatology 2003;38:1449–1457.

24. Scheuer PJ. Liver biopsy size matters in chronic hepatitis: bigger is better. Hepatology 2003;38:1356–1358.

25. Eisenberg E, Konopniki M, Veitsman E, Kramskay R, Gaitini D, Baruch Y. Prevalence and characteristics of pain induced by percutaneous liver biopsy. Anesth Analg 2003;96:1392–1396, table of contents.

26. Fernandez-Salazar L, Velayos B, Aller R, Lozano F, Garrote JA, Gonzalez JM. Percutaneous liver biopsy: patients' point of view. Scand J Gastroenterol 2011;5521:1–5.

27. Bonny C, Rayssiguier R, Ughetto S, et al. Medical practices and expectations of general practitioners in relation to hepatitis C virus infection in the Auvergne region. Gastroenterol Clin Biol 2003;27: 1021–1025.

28. Lee YA, Wallace MC, Friedman SL. Pathobiology of liver fibrosis: a translational success story. Gut 2015;64:830–841.

29. Chung RT, Davis GL, Jensen DM, et al. Hepatitis C guidance: AASLD-IDSA recommendations for testing, managing, and treating adults infected with hepatitis C virus. Hepatology 2015;62:932–954.

30. Lok ASF, McMahon BJ, Brown RS, et al. Antiviral therapy for chronic hepatitis B viral infection in adults: A systematic review and meta-analysis. Hepatology 2016;63:284–306.

31. Brancatelli G, Federle MP, Ambrosini R, et al. Cirrhosis: CT and MR imaging evaluation. Eur J Radiol 2007;61:57–69.

32. Numminen K, Tervahartiala P, Halavaara J, Isoniemi H, Höckerstedt K. Non-invasive diagnosis of liver cirrhosis: magnetic resonance imaging presents special features. Scand J Gastroenterol 2005;40:76–82.

33. Colli A, Fraquelli M, Andreoletti M, Marino B, Zuccoli E, Conte D. Severe liver fibrosis or cirrhosis: accuracy of US for detection—analysis of 300 cases. Radiology 2003;227:89–94.

34. Aubé C, Oberti F, Korali N, et al. Ultrasonographic diagnosis of hepatic fibrosis or cirrhosis. J Hepatol 1999;30:472–478.

35. Hung CH, Lu SN, Wang JH, et al. Correlation between ultrasonographic and pathologic diagnoses of hepatitis B and C virus-related cirrhosis. J Gastroenterol 2003;38:153–157.

36. Berzigotti A, Abraldes JG, Tandon P, et al. Ultrasonographic evaluation of liver surface and transient elastography in clinically doubtful cirrhosis. J Hepatol 2010;52:846–853.

37. Ohtomo K, Baron RL, Dodd GD, et al. Confluent hepatic fibrosis in advanced cirrhosis: appearance at CT. Radiology 1993;188:31–35.

38. Brancatelli G, Baron RL, Federle MP, Sparacia G, Pealer K. Focal confluent fibrosis in cirrhotic liver: Natural history studied with serial CT. Am J Roentgenol 2009;192:1341–1347.

39. Zeitoun D, Brancatelli G, Colombat M, et al. Congenital hepatic fibrosis: CT findings in 18 adults. Radiology 2004;231:109–116.

40. Rustogi R, Horowitz J, Harmath C, et al. Accuracy of MR elastography and anatomic MR imaging features in the diagnosis of severe hepatic fibrosis and cirrhosis. J Magn Reson Imaging 2012;35:1356–1364.

41. Venkatesh SK, Yin M, Takahashi N, Glockner JF, Talwalkar JA, Ehman RL. Non-invasive detection of liver fibrosis: MR imaging features vs. MR elastography. Abdom Imaging 2015;40:766–775.

42. Kudo M, Zheng RQ, Kim SR, et al. Diagnostic accuracy of imaging for liver cirrhosis compared to histologically proven liver cirrhosis. Intervirology 2008;51(Suppl 1):17–26.

43. Bahl G, Cruite I, Wolfson T, et al. Noninvasive classification of hepatic fibrosis based on texture parameters from double contrast-enhanced magnetic resonance images. J Magn Reson Imaging 2012;36:1154–1161.

44. Toyoda H, Kumada T, Kamiyama N, et al. B-mode ultrasound with algorithm based on statistical analysis of signals: evaluation of liver fibrosis in patients with chronic hepatitis C. AJR Am J Roentgenol 2009;193:1037–1043.

45. Vicas C, Lupsor M, Badea R, Nedevschi S. Usefulness of textural analysis as a tool for noninvasive liver fibrosis staging. J Med Ultrason 2011;38:105–117.

46. Kvostikov AV., Krylov AS, Kamalov UR. Ultrasound image texture analysis for liver fibrosis stage diagnostics. Program Comput Softw 2015; 41:273–278.

47. Basset O, Duboeuf F, Delhay B, Brusseau E, Cachard C, Tasu JP. Texture analysis of ultrasound liver images with contrast agent to characterize the fibrosis stage. Proc IEEE Ultrason Symp 2008:24–27.

48. Wang Y, Itow K, Taniguchi N, et al. Studies on tissue characterization by texture analysis with co-occurrence matrix method using ultrasonography and CT imaging. J Med Ultrason 2002;29:825–837.

49. Daginawala N, Li B, Buch K, et al. Using texture analyses of contrast enhanced CT to assess hepatic fibrosis. Eur J Radiol 2015;85:511–517.

50. Kayaalti Ö, Aksebzeci BH, Karahan IÖ, et al. Liver fibrosis staging using CT image texture analysis and soft computing. Appl Soft Comput 2014;25:399–413.

51. Varenika V, Fu Y, Maher JJ, et al. Hepatic fibrosis: evaluation with semiquantitative contrast-enhanced CT. Radiology 2013;266:151–158.

52. Mahmoud-Ghoneim D, Amin A, Corr P. MRI-based texture analysis: a potential technique to assess protectors against induced-liver fibrosis in rats. Radiol Oncol 2009;43:30–40.

53. House MJ, Bangma SJ, Thomas M, et al. Texture-based classification of liver fibrosis using MRI. J Magn Reson Imaging 2015;41:322–328.

54. Yu H, Buch K, Li B, et al. Utility of texture analysis for quantifying hepatic fibrosis on proton density MRI. J Magn Reson Imaging 2015; 42:1259–1265.

55. Aguirre DA, Behling CA, Alpert E, Hassanein TI, Sirlin CB. Liver fibrosis: noninvasive diagnosis with double contrast material-enhanced MR imaging. Radiology 2006;239:425–437.

56. Yokoo T, Wolfson T, Iwaisako K, et al. Evaluation of liver fibrosis using texture analysis on combined-contrast-enhanced magnetic resonance images at 3.0T. Biomed Res Int 2015;2015(Cld).

57. Kato H, Kanematsu M, Zhang X, et al. Computer-aided diagnosis of hepatic fibrosis: Preliminary evaluation of mri texture analysis using the finite difference method and an artificial neural network. Am J Roentgenol 2007;189:117–122.

58. Vasanawala SS, Nguyen K-L, Hope MD, et al. Safety and technique of ferumoxytol administration for MRI. Magn Reson Med 2016;75:2107–2111.

59. Tang A, Cloutier G, Szeverenyi NM, Sirlin CB. Ultrasound elastography and MR elastography for assessing liver fibrosis: Part 2, diagnostic performance, confounders, and future directions. Am J Roentgenol 2015;205:33–40.

60. Castéra L, Vergniol J, Foucher J, et al. Prospective comparison of transient elastography, Fibrotest, APRI, and liver biopsy for the assessment of fibrosis in chronic hepatitis C. Gastroenterology 2005; 128:343–350.

61. Friedrich-Rust M, Wunder K, Kriener S, et al. Liver fibrosis in viral hepatitis: noninvasive assessment with acoustic radiation force impulse imaging versus transient elastography. Radiology 2009;252:595–604.

62. Bavu É, Gennisson JL, Couade M, et al. Noninvasive in vivo liver fibrosis evaluation using supersonic shear imaging: a clinical study on 113 hepatitis C virus patients. Ultrasound Med Biol 2011;37:1361–1373.

63. Yin M, Talwalkar JA, Glaser KJ, et al. Assessment of hepatic fibrosis with magnetic resonance elastography. Clin Gastroenterol Hepatol 2007;5:1207–1213.

64. Asbach P, Klatt D, Schlosser B, et al. Viscoelasticity-based staging of hepatic fibrosis with multifrequency MR elastography. Radiology 2010;257.

65. Kazemirad S, Zhang E, Nguyen BN, et al. Detection of steatohepatitis in a rat model by using spectroscopic shear-wave US elastography. Radiology 2017 [Epub ahead of print].

66. Kaminuma C, Tsushima Y, Matsumoto N, Kurabayashi T, Taketomi-Takahashi A, Endo K. Reliable measurement procedure of virtual touch tissue quantification with acoustic radiation force impulse imaging. J Ultrasound Med 2011;30:745–751.

67. Iredale JP. Models of liver fibrosis: Exploring the dynamic nature of inflammation and repair in a solid organ. J Clin Invest 2007;117:539–548.

68. Karlas T, Pfrepper C, Troeltzsch M, Wiegand J, Keim V. Acoustic radiation force impulse liver stiffness measurement: interlobe differences demand standardized examination procedures. Eur J Gastroenterol Hepatol 2010;22:1387.

69. Mederacke I, Wursthorn K, Kirschner J, et al. Food intake increases liver stiffness in patients with chronic or resolved hepatitis C virus infection. Liver Int 2009;29:1500–1506.

70. Yin M, Talwalkar JA, Glaser KJ, et al. Dynamic postprandial hepatic stiffness augmentation assessed with MR elastography in patients with chronic liver disease. Am J Roentgenol 2011;197:64–70.

71. Bamber J, Cosgrove D, Dietrich CF, et al. Speeds of sound waves and shear-waves. Ultraschall der Medizin 2013;34:1–3.

72. Sandrin L, Fourquet B, Hasquenoph JM, et al. Transient elastography: a new noninvasive method for assessment of hepatic fibrosis. Ultrasound Med Biol 2003;29:1705–1713.

73. Nightingale K, Scott Soo M, Nightingale R, Trahey G. Acoustic radiation force impulse imaging: in vivo demonstration of clinical feasibility. Ultrasound Med Biol 2002;28:227–235.

74. Bercoff J, Tanter M, Fink M. Supersonic shear imaging: a new technique. IEEE Trans Ultrason Ferroelectr Freq Control 2004;51:396–409.

75. Zhang E, Wartelle-Bladou C, Lepanto L, Lachaine J, Cloutier G, Tang A. Cost-utility analysis of nonalcoholic steatohepatitis screening. Eur Radiol 2015;25:3282–3294.

76. Myers RP, Pomier-Layrargues G, Kirsch R, et al. Feasibility and diagnostic performance of the FibroScan XL probe for liver stiffness measurement in overweight and obese patients. Hepatology 2012;55:199–208.

77. Talwalkar JA, Kurtz DM, Schoenleber SJ, West CP, Montori VM. Ultrasound-based transient elastography for the detection of hepatic fibrosis: Systematic review and meta-analysis. Clin Gastroenterol Hepatol 2007;5:1214–1220.

78. Friedrich-Rust M, Ong MF, Martens S, et al. Performance of transient elastography for the staging of liver fibrosis: a meta-analysis. Gastroenterology 2008;134:960–974.

79. Tsochatzis EA, Gurusamy KS, Ntaoula S, Cholongitas E, Davidson BR, Burroughs AK. Elastography for the diagnosis of severity of fibrosis in chronic liver disease: A meta-analysis of diagnostic accuracy. J Hepatol 2011;54:650–659.

80. Bota S, Herkner H, Sporea I, et al. Meta-analysis: ARFI elastography versus transient elastography for the evaluation of liver fibrosis. Liver Int 2013;33:1138–1147.

81. Friedrich-Rust M, Nierhoff J, Lupsor M, et al. Performance of Acoustic Radiation Force Impulse imaging for the staging of liver fibrosis: A pooled meta-analysis. J Viral Hepat 2012;19:212–219.

82. Tse ZTH, Janssen H, Hamed A, Ristic M, Young I, Lamperth M. Magnetic resonance elastography hardware design: a survey. J Eng Med 2009;223:497–514.

83. Asbach P, Klatt D, Hamhaber U, Somasundaram R. Assessment of liver viscoelasticity using multifrequency MR elastography. Magn Reson Med 2008;379:373–379.

84. Huwart L, Sempoux C, Salameh N, et al. Liver fibrosis: noninvasive assessment with MR elastography versus aspartate aminotransferase-to-platelet ratio index. Radiology 2007;245.

85. Sinkus R, Tanter M, Catheline S, et al. Imaging anisotropic and viscous properties of breast tissue by magnetic resonance-elastography. Magn Reson Med 2005;53:372–387.

86. Muthupillai R, Lomas DJ, Rossman PJ, Greenleaf JF, Manduca A, Ehman RL. Magnetic resonance elastography by direct visualization of propagating acoustic strain waves. Science 1995;269:1854–1857.

87. Klatt D, Asbach P, Rump J, et al. In vivo determination of hepatic stiffness using steady-state free precession magnetic resonance elastography. Invest Radiol 2006;41:841–848.

88. Kwon OI, Park C, Nam HS, et al. Shear modulus decomposition algorithm in magnetic resonance elastography. IEEE Trans Med Imaging 2009;28:1526–1533.

89. Dunn T, Majumdar S. Comparison of motion encoding waveforms for magnetic resonance elastography at 3T. Conf Proc IEEE Eng Med Biol Soc 2005;7:7405–7408.

90. Herzka DA, Kotys MS, Sinkus R, Pettigrew RI, Gharib AM. Magnetic resonance elastography in the liver at 3 Tesla using a second harmonic approach. Magn Reson Med 2009;62:284–291.

91. Manduca A, Oliphant TE, Dresner MA, et al. Magnetic resonance elastography: Non-invasive mapping of tissue elasticity. Med Image Anal 2001;5:237–254.

92. Dzyubak B, Venkatesh SK, Manduca A, Glaser KJ, Ehman RL. Automated liver elasticity calculation for MR elastography. J Magn Reson Imaging 2016;43:1055–1063.

93. Venkatesh SK, Ehman RL. Magnetic resonance elastography of liver. Magn Reson Imaging Clin N Am 2014;22:433–446.

94. Trout AT, Serai S, Mahley AD, et al. Liver stiffness measurements with MR elastography: Agreement and repeatability across imaging systems, field strengths and pulse sequences. Radiology 2016 [Epub ahead of print].

95. Serai SD, Yin M, Wang H, Ehman RL, Podberesky DJ. Cross-vendor validation of liver magnetic resonance elastography. Abdom Imaging 2015;40:789–794.

96. Wang QB, Zhu H, Liu HL, Zhang B. Performance of magnetic resonance elastography and diffusion-weighted imaging for the staging of hepatic fibrosis: A meta-analysis. Hepatology 2012;56:239–247.

97. Singh S, Venkatesh SK, Wang Z, et al. Diagnostic performance of magnetic resonance elastography in staging liver fibrosis: A systematic review and meta-analysis of individual participant data. Clin Gastroenterol Hepatol 2015;13:440–451.

98. Guo Y, Parthasarathy S, Goyal P, McCarthy RJ, Larson AC, Miller FH. Magnetic resonance elastography and acoustic radiation force impulse for staging hepatic fibrosis: a meta-analysis. Abdom Imaging 2015;40:818–834.

99. Huwart L, Sempoux C, Vicaut E, et al. Magnetic resonance elastography for the noninvasive staging of liver fibrosis. Gastroenterology 2008;135:32–40.

100. Yoon JH, Lee JM, Joo I, et al. Hepatic fibrosis: prospective comparison of MR elastography and US shear wave elastography for evaluation. Radiology 2014;273:132000.

101. Tang A, Cloutier G, Szeverenyi NM, Sirlin CB. Ultrasound elastography and MR elastography for assessing liver fibrosis: Part 1, principles and techniques. AJR Am J Roentgenol 2015;205:22–32.

102. Yin M, Glaser KJ, Talwalkar JA, Chen J, Manduca A, Ehman RL. Hepatic MR Elastography: Clinical Performance in a Series of 1377 Consecutive Examinations. Radiology 2016;278:114–124.

103. Venkatesh SK, Yin M, Ehman RL. Magnetic resonance elastography of liver: technique, analysis, and clinical applications. J Magn Reson Imaging 2013;37:544–555.

104. Singh S, Venkatesh SK, Loomba R, et al. Magnetic resonance elastography for staging liver fibrosis in non-alcoholic fatty liver disease: a diagnostic accuracy systematic review and individual participant data pooled analysis. Eur Radiol 2016;26:1431–1440.

105. Watanabe H, Kanematsu M, Kitagawa T, et al. MR elastography of the liver at 3 T with cine-tagging and bending energy analysis: Preliminary results. Eur Radiol 2010;20:2381–2389.

106. Osman NF, Faranesh a Z, Mcveigh ER, Prince JL. Tracking cardiac motion using cine harmonic phase (HARP) MRI. Magn Reson Med 1999;42:1048–1060.

107. Barajas J, Garcia-Barnés J, Carreras F, Pujadas S, Radeva P. Angle images using Gabor filters in cardiac tagged MRI. Front Artif Intell Appl 2005;131:107–114.

108. Chung S, Kim KE, Park MS, Bhagavatula S, Babb J, Axel L. Liver stiffness assessment with tagged MRI of cardiac-induced liver motion in cirrhosis patients. J Magn Reson Imaging 2014;39:1301–1307.

109. Mannelli L, Wilson GJ, Dubinsky TJ, et al. Assessment of the liver strain among cirrhotic and normal livers using tagged MRI. J Magn Reson Imaging 2012;36:1490–1495.

110. Harouni AA, Gharib AM, Osman NF, Morse C, Heller T, Abd-Elmoniem KZ. Assessment of liver fibrosis using fast strain-encoded MRI driven by inherent cardiac motion. Magn Reson Med 2014 [Epub ahead of print].

111. Gilani IA, Sepponen R. Quantitative rotating frame relaxometry methods in MRI. NMR Biomed 2016;841–861.

112. Wang Y-X, Yuan J, Chu E, et al. T1 ρ MR imaging is sensitive to evaluate liver fibrosis: an experimental study in a rat biliary duct ligation model. Radiology 2011;259:712–719.

113. Yuan J, Zhao F, Griffith JF, Chan Q, Wang Y-XJ. Optimized efficient liver T1ρ mapping using limited spin lock times. Phys Med Biol 2012;57:1631–1640.

114. Allkemper T, Sagmeister F, Cicinnati V, et al. Evaluation of fibrotic liver disease with whole-liver T1ρ MR imaging: a feasibility study at 1.5 T. Radiology 2014;271:408–415.

115. Singh A, Reddy D, Haris M, et al. T1ρ MRI of healthy and fibrotic human livers at 1.5 T. J Transl Med 2015;13:292.

116. Jiang J, Huang B, Bin G, Chen S, Feng F, Zou L. An experimental study on the assessment of rabbit hepatic fibrosis by using magnetic resonance T1ρ imaging. Magn Reson Imaging 2015;34:308–311.

117. Zhao F, Deng M, Yuan J, Teng GJ, Ahuja AT, Wang YXJ. Experimental evaluation of accelerated T1rho relaxation quantification in human liver using limited spin-lock times. Korean J Radiol 2012;13: 736–742.

118. Deng M, Zhao F, Yuan J, Ahuja AT, Wang YXJ. Liver T1ρ MRI measurement in healthy human subjects at 3 T: A preliminary study with a two-dimensional fast-field echo sequence. Br J Radiol 2012;85.

119. Rauscher I, Eiber M, Ganter C, et al. Evaluation of T1ρ as a potential MR biomarker for liver cirrhosis: Comparison of healthy control subjects and patients with liver cirrhosis. Eur J Radiol 2014;83:900–904.

120. Takayama Y, Nishie A, Asayama Y, et al. T1ρ relaxation of the liver: A potential biomarker of liver function. J Magn Reson Imaging 2014; 195:188–195.

121. Le Bihan D. Molecular diffusion, tissue microdynamics and microstructure. NMR Biomed 1995;8:375–386.

122. Le Bihan D, Breton E, Lallemand D, Aubin M-L, Vignaud J, Laval-Jeantet M. Separation of diffusion and perfusion in intravoxel incoherent motion MR imaging. Radiology 1988;168:497–505.

123. Taouli B, Koh D-M. Diffusion-weighted MR imaging of the liver. Radiology 2010;254:47–66.

124. Bakan AA, Inci E, Bakan S, Gokturk S, Cimilli T. Utility of diffusion-weighted imaging in the evaluation of liver fibrosis. Eur Radiol 2012; 22:682–687.

125. Bonekamp S, Torbenson MS, Kamel IR. Diffusion-weighted magnetic resonance imaging for the staging of liver fibrosis. J Clin Gastroenterol 2011;45:885–892.

126. Koinuma M, Ohashi I, Hanafusa K, Shibuya H. Apparent diffusion coefficient measurements with diffusion-weighted magnetic resonance imaging for evaluation of hepatic fibrosis. J Magn Reson Imaging 2005;22:80–85.

127. Sandrasegaran K, Akisik FM, Lin C, et al. Value of diffusion-weighted MRI for assessing liver fibrosis and cirrhosis. Am J Roentgenol 2009; 193:1556–1560.

128. Taouli B, Tolia AJ, Losada M, et al. Diffusion-weighted MRI for quantification of liver fibrosis: Preliminary experience. Am J Roentgenol 2007;189:799–806.

129. Annet L, Peeters F, Abarca-Quinones J, Leclercq I, Moulin P, Van Beers BE. Assessment of diffusion-weighted MR imaging in liver fibrosis. J Magn Reson Imaging 2007;25:122–128.

130. Luciani A, Vignaud A, Cavet M, et al. Liver cirrhosis: intravoxel incoherent motion MR imaging—pilot study. Radiology 2008;249:891–899.

131. Chow AM, Gao DS, Fan SJ, et al. Liver fibrosis: An intravoxel incoherent motion (IVIM) study. J Magn Reson Imaging 2012;36:159–167.

132. Hu G, Chan Q, Quan X, et al. Intravoxel incoherent motion MRI evaluation for the staging of liver fibrosis in a rat model. J Magn Reson Imaging 2014;42:331–339.

133. Patel J, Sigmund EE, Rusinek H, Oei M, Babb JS, Taouli B. Diagnosis of cirrhosis with intravoxel incoherent motion diffusion MRI and dynamic contrast-enhanced MRI alone and in combination: Preliminary experience. J Magn Reson Imaging 2010;31:589–600.

134. Yoon JH, Lee JM, Baek JH, et al. Evaluation of hepatic fibrosis using intravoxel incoherent motion in diffusion-weighted liver MRI. J Comput Assist Tomogr 2014;38:110–116.

135. Friedman SL. Mechanisms of hepatic fibrogenesis. Gastroenterology 2008;134:1655–1669.

136. Girometti R, Furlan A, Esposito G, et al. Relevance of b-values in evaluating liver fibrosis: A study in healthy and cirrhotic subjects using two single-shot spin-echo echo-planar diffusion-weighted sequences. J Magn Reson Imaging 2008;28:411–419.

137. Ozkurt H, Keskiner F, Karatag O, Alkim C, Erturk SM, Basak M. Diffusion weighted MRI for hepatic fibrosis: Impact of b-value. Iran J Radiol 2014;11:1–8.

138. Bülow R, Mensel B, Meffert P, Hernando D, Evert M, Kühn JP. Diffusion-weighted magnetic resonance imaging for staging liver fibrosis is less reliable in the presence of fat and iron. Eur Radiol 2013;23: 1281–1287.

139. Materne R, van Beers BE, Smith a M, et al. Non-invasive quantification of liver perfusion with dynamic computed tomography and a dual-input one-compartmental model. Clin Sci (Lond) 2000;99:517–525.

140. Khalifa F, Soliman A, El-baz A, et al. Models and methods for analyzing DCE-MRI: A review. Med Phys 2014;41:1–32.

141. Hagiwara M, Rusinek H, Lee VS, et al. Advanced liver fibrosis: diagnosis with 3D whole-liver. Radiology 2008;246:926–934.

142. Aronhime S, Calcagno C, Jajamovich GH, et al. DCE-MRI of the liver: effect of linear and nonlinear conversions on hepatic perfusion quantification and reproducibility. J Magn Reson Imaging 2014;40: 90–98.

143. Ou HY, Bonekamp S, Bonekamp D, et al. MRI arterial enhancement fraction in hepatic fibrosis and cirrhosis. Am J Roentgenol 2013;201: 596–602.

144. Bonekamp D, Bonekamp S, Geiger B, Kamel IR. An elevated arterial enhancement fraction is associated with clinical and imaging indices of liver fibrosis and cirrhosis. J Comput Assist Tomogr 2012;36:681–689.

145. Kim H, Booth CJ, Pinus AB, et al. Induced hepatic fibrosis in rats: hepatic steatosis, macromolecule content, perfusion parameters, and their correlations—preliminary MR imaging in rats. Radiology 2008; 247:696–705.

146. Seale MK, Catalano OA, Saini S, Hahn PF, Sahani DV. Hepatobiliary-specific MR contrast agents: role in imaging the liver and biliary tree. Radiographics 2009;29:1725–1748.

147. Verloh N, Utpatel K, Haimerl M, et al. Liver fibrosis and Gd-EOB-DTPA-enhanced MRI: A histopathologic correlation. Nat Sci Reports 2015:1–10.

148. Watanabe H, Kanematsu M, Goshima S, et al. Staging hepatic fibrosis: comparison of gadoxetate disodium-enhanced and diffusion-weighted MR imaging — preliminary observations. Radiology 2011; 259.

149. Feier D, Balassy C, Bastati N, Stift J, Badea R, Ba-Ssalamah A. Liver fibrosis: histopathologic and biochemical influences on diagnostic efficacy of hepatobiliary contrast-enhanced MR imaging in staging. Radiology 2013;269:460–468.

150. Kumazawa K, Edamoto Y, Yanase M, Nakayama T. Liver analysis using gadolinium-ethoxybenzyl-diethylenetriamine pentaacetic acid-enhanced magnetic resonance imaging: Correlation with histological grading and quantitative liver evaluation prior to hepatectomy. Hepatol Res 2012;42:1081–1088.

151. Motosugi U, Ichikawa T, Oguri M, et al. Staging liver fibrosis by using liver-enhancement ratio of gadoxetic acid-enhanced MR imaging: Comparison with aspartate aminotransferase-to-platelet ratio index. Magn Reson Imaging 2011;29:1047–1052.

152. Goshima S, Kanematsu M, Watanabe H, et al. Gd-EOB-DTPA-enhanced MR imaging: Prediction of hepatic fibrosis stages using liver contrast enhancement index and liver-to-spleen volumetric ratio. J Magn Reson Imaging 2012;36:1148–1153.

153. Xie S, Sun Y, Wang L, Yang Z, Luo J, Wang W. Assessment of liver function and liver fibrosis with dynamic Gd-EOB-DTPA-enhanced MRI. Acad Radiol 2015;22:460–466.

154. Okuaki T, Morita K, Namimoto T, et al. Assessment of the Hepatocyte Fraction for estimation of liver function. In: Proc 23rd Annual Meeting ISMRM, Toronto; 2015.p 384.

155. Okuaki T, Morita K, Namimoto T, et al. Comparison of the hepatocyte fraction and conventional image based methods for the estimation of liver function. In: Proc 24th Annual Meeting ISMRM, Singapore; 2016.

156. Chow AM, Gao DS, Fan SJ, et al. Measurement of liver T1 and T2 relaxation times in an experimental mouse model of liver fibrosis. J Magn Reson Imaging 2012;36:152–158.

157. Haimerl M, Verloh N, Zeman F, et al. Assessment of clinical signs of liver cirrhosis using T1 mapping on Gd-EOB-DTPA-enhanced 3T MRI. PLoS One 2013;8:1–8.

158. Balassy C, Feier D, Peck-Radosavljevic M, et al. Susceptibility-weighted MR imaging in the grading of liver fibrosis: a feasibility study. Radiology 2014;270:149–158.

159. Feier D, Balassy C, Bastati N, Fragner R, Wrba F, Ba-Ssalamah A. The diagnostic efficacy of quantitative liver MR imaging with diffusion-weighted, SWI, and hepato-specific contrast-enhanced sequences in staging liver fibrosis — a multiparametric approach. Eur Radiol 2015;26:539–546.

160. Caravan P, Das B, Dumas S, et al. Collagen-targeted MRI contrast agent for molecular imaging of fibrosis. Angew Chem Int Ed 2007; 46:8171–8173.

161. Farrar CT, Deperalta DK, Day H, et al. 3D molecular MR imaging of liver fibrosis and response to rapamycin therapy in a bile duct ligation rat model. J Hepatol 2015;63:689–696.

162. Fuchs BC, Wang H, Yang Y, et al. Molecular MRI of collagen to diagnose and stage liver fibrosis. J Hepatol 2013;59:992–998.

163. Polasek M, Fuchs BC, Uppal R, et al. Molecular MR imaging of liver fibrosis: A feasibility study using rat and mouse models. J Hepatol 2012;57:549–555.

164. Kishore R, Loomba R, Sterling RK. Editorial: a new spin on magnetic resonance elastography. Am J Gastroenterol 2016;111:834–837.

165. Salameh N, Sarracanie M, Armstrong BD, Rosen MS, Comment A. Overhauser-enhanced magnetic resonance elastography. NMR Biomed 2016;29:607–613.

166. Yin Z, Magin RL, Klatt D. Simultaneous MR elastography and diffusion acquisitions: Diffusion-MRE (dMRE). Magn Reson Med 2014;71: 1682–1688.

167. Salameh N, Larrat B, Abarca-Quinones J, et al. Early detection of steatohepatitis in fatty rat liver by using MR elastography. Radiology 2009;253:90–97.

168. Chen J, Talwalkar JA, Yin M, Glaser KJ, Sanderson SO, Ehman RL. Early detection of nonalcoholic steatohepatitis in patients with nonalcoholic fatty liver disease by using MR elastography. Radiology 2011;259:749–756.

169. Banerjee R, Pavlides M, Tunnicliffe EM, et al. Multiparametric magnetic resonance for the non-invasive diagnosis of liver disease. J Hepatol 2014;60:69–77.

170. Zhang Y, Zhang XM, Prowda JC, et al. Changes in hepatic venous morphology with cirrhosis on MRI. J Magn Reson Imaging 2009;29: 1085–1092.

171. Choi YR, Lee JM, Yoon JH, Han JK, Choi BI. Comparison of magnetic resonance elastography and gadoxetate disodium-enhanced magnetic resonance imaging for the evaluation of hepatic fibrosis. Invest Radiol 2013;48:607–613.